Received: 13 November 2020 | Revised: 24 May 2021 | Accepted: 26 May 2021

DOI: 10.1111/jmg.12621

ORIGINAL ARTICLE

Journal of METAMORPHIC GEOLOGY WILEY

Deep subduction, melting, and fast cooling of metapelites from the Cima Lunga Unit, Central Alps

Francesca Piccoli | **Pierre Lanari** | **Jörg Hermann** | **Thomas Pettke**

Institute of Geological Sciences, University of Bern, Bern, Switzerland

Correspondence
Francesca Piccoli, Institute of Geological Sciences, University of Bern, Bern 1+3, 3012, Switzerland.
Email: francesca.piccoli@geo.unibe.ch

Handling Editor: Bernardo Cesare

Abstract

The Cima Lunga unit in the Central Alps is dominated by quartzofeldspathic gneisses with subordinate mafic, ultramafic, and metacarbonate rocks. Only mafic and ultramafic lithologies were thought to preserve clear evidence of Alpine high-*P* metamorphism. This led to the questions of whether the different rock types were subducted and exhumed as a coherent unit or underwent different pressure–temperature (*P–T*) histories. New petrological and geochemical data from a metapelite associated with garnet peridotite from Cima di Gagnone (Cima Lunga unit, Switzerland) were obtained using major and trace element mapping. Complex zoning patterns in garnet and white mica are observed. In particular, high Ti content in phengite and increasing P, Zr, and HREE contents in pyrope-rich garnet indicate that this metapelite underwent high-*P* and high-*T* (*HP–HT*) metamorphism involving fluid-fluxed partial melting. A *P–T* path is reconstructed by combining textural analysis with petrological–geochemical data and thermodynamic simulations. We show that the mineral record preserves an evolution from prograde to *HP–HT* peak conditions (2.7 ± 0.1 GPa and 800°C) followed by near-isobaric cooling (~2.5 GPa and 700–750°C) prior to decompression (1.0 GPa and ~620°C). The reconstructed *P–T* path suggests that the studied metapelites were subducted to depths where the slab gets heated by proximity to asthenospheric mantle related to slab break-off. This heating resulted in the dehydration of chlorite- to garnet peridotite and the liberated fluids triggered partial melting in the associated metapelites, which might have favoured the fast exhumation of the entire Cima Lunga unit. Metapelites and garnet peridotite from Cima di Gagnone underwent a common prograde to peak and retrograde *P–T* path without significant tectonic pressure difference between the different lithologies, and deviation from lithostatic pressure is excluded. Lastly, the peak metamorphic conditions of metapelite from Cima di Gagnone are comparable with *P–T* estimates of ultramafic lithologies from the southern Adula nappe and the Dascio Bellinzona zone, thus opening new scenarios for the geodynamic interpretation of the Central Alps.

KEYWORDS

Central European Alps, Cima Lunga unit, high-*P* metamorphism, subduction plate interface

1 | INTRODUCTION

The slab–mantle wedge interface is a site of important tectonic processes. The nature of this interface can determine the exhumation, or not, of high-*P* (HP) to ultra high pressure (UHP) rocks and, ultimately, control the structure of a collisional orogenic belt. Different models of geometry and driving forces for the exhumation of *(U)HP* units are proposed in the literature (Hacker & Gerya, 2013). The exhumation of *(U)HP* rocks has been attributed to (a) continuous return flow in low density channels, favoured by buoyant carriers such as serpentinites or metasediments (England & Holland, 1979; Gerya et al., 2002; Guillot et al., 2001; Hermann et al., 2000; Lang & Gilotti, 2015); (b) upward flow of individual buoyant rock units within a denser material (i.e. Stokes flow, Burov et al., 2001; Hermann et al., 2000); (c) lithospheric extension caused by slab rollback and exhumation along reactivated pre-existing structures (Beltrando et al., 2010, 2014); and (d) negative buoyancy driven downward removal of overburden and consequent diapiric extrusion of the underlying *(U)HP* rocks (Froitzheim et al., 2003; Majka et al., 2014). Mechanism (a) and (b) results in a 'tectonic mélange' consisting of fragments with contrasting *P–T–t* paths that, potentially, experienced repeated subduction–exhumation cycles within a few million years (Gerya et al., 2002; Rubatto et al., 2011). Field and geochemical observations in favour of this model are (a) the relatively small volume of rocks within the same tectonic unit that actually displays (U)HP assemblages (Jolivet et al., 2005; Krebs et al., 2011), and (b) scattered isotopic ages related to HP conditions (Federico et al., 2007). In contrast, mechanism (c) involves the exhumation of coherent units (i.e. with continuous metamorphic gradients and ages; Angiboust et al., 2009; Beltrando et al., 2014; Vitale Brovarone et al., 2011), possibly coinciding with the initiation of continental crust subduction (Agard et al., 2009; Chemenda et al., 1995; Harlow et al., 2004; Warren et al., 2008). Mechanism (d), slab extraction, explains the emplacement of (U)HP unit in a pile of LP nappes in the particular geodynamic setting where two neighbouring subduction zones with same dipping direction interact (Froitzheim et al., 2003). All these models assume that the pressure obtained by phase equilibria is close to lithostatic pressures and that the contribution of deviatoric stress is negligible. The lithostatic pressure paradigm allows the metamorphic pressure to be converted directly into burial depth. Alternative models invoke tectonic overpressure generated during crustal shortening for explaining the disparate presence of mafic and ultramafic (U)HP rocks within a quartzofeldspatic basement without evidence for HP metamorphism (Pleuger & Podladchikov, 2014; Schenker et al., 2015; Schmalholz & Duretz, 2015; Schmalholz et al., 2014). An important aspect of the overpressure model is that different rock types should record different peak pressure conditions (Luisier et al., 2019; Moulas et al., 2013).

The Cima Lunga unit in the eastern Central Alps is a mixture of mafic, ultramafic, metacarbonate, and felsic rock types that has been interpreted as a subduction channel-tectonic mélange because of the presence of HP mafic eclogite and UHP garnet peridotite embedded within the lower pressure quartzofeldspatic basement (Trommsdorff, 1990). A large number of subsequent studies proposed that this unit represents a mélange of rocks with different palaeogeographic provenances and/or different subduction histories (Berger et al., 2005; Brouwer et al., 2005; Engi et al., 2001; Grond et al., 1995; Pfiffner, 1999; Toóth et al., 2000; Trommsdorff, 1990). Other studies proposed a more coherent metamorphic history at least since peak pressure conditions (Carry et al., 2009; Cavargna-Sani et al., 2014; Dale & Holland, 2003; Heinrich, 1982; Herwartz et al., 2011; Nagel, 2008). Alternatively, recent studies suggest that the *(U)HP* metamorphism recorded by mafic and ultramafic lenses occurred at the base of thickened continental crust as a result of episodic and local tectonic overpressure (Pleuger & Podladchikov, 2014; Schenker et al., 2015). A major challenge for the tectonic interpretation of the Cima Lunga unit is that the reconstruction of its metamorphic history is often hampered by different degrees of re-equilibration between mafic, ultramafic and felsic lithologies (Heinrich, 1982), with a pervasive recrystallization of the gneisses during the amphibolite facies Lepontine metamorphism after the HP event (Boston et al., 2017; Engi et al., 2001). Deciphering the detailed *P–T* path preserved in mineral assemblages is crucial for the understanding of the geological processes taking place in the subduction plate interface. In particular, the process capable of explaining the exhumation of very dense rocks, such as garnet peridotites, has yet to be thoroughly understood.

In this study, we investigate metapelitic rocks associated with the garnet peridotites from Cima di Gagnone, in the Cima Lunga unit. We use petrological, geochemical, and theoretical considerations to reconstruct the metamorphic *P–T* evolution of the metapelites. We show that multiple metamorphic stages preserve prograde to HP–HT peak and retrograde (amphibolite facies) partial equilibration, in line with the conditions recorded by the mafic and ultramafic lenses. Our findings suggest that the mafic, ultramafic, and associated felsic lithologies from Cima di Gagnone were subducted and exhumed as a coherent unit without significant metamorphic pressure variation despite the presence of mechanically heterogeneous rocks. Considering also other literature, we propose that the Cima Lunga unit is a fragment of the hyperextended European continental margin of the Piemonte–Ligurian ocean.

2 | GEOLOGICAL CONTEXT

The Central Alps represent the internal part of the Alpine collisional orogen, where regional amphibolite facies metamorphism postdates the stacking of nappes (Engi et al., 2001). An Oligocene thermal pulse mainly affected the southern part of the Central Alps, where migmatites are widespread (Todd & Engi, 1997). Peak amphibolite facies *P–T* ranges from 500 to 550°C and 0.7 GPa in the north and west areas, to ~675°C and 0.55–0.45 GPa southward, towards the Insubric line (Todd & Engi, 1997). Peak amphibolite facies metamorphic ages are 30–22 Ma (U–Pb zircon ages, Boston et al., 2017; Rubatto et al., 2009).

The Cima Lunga unit is located in the Central Alps and makes part of the Penninic nappe system. It consists of a crystalline continental basement with pelitic, mafic, and granitoid rocks, partially overlain by a Mesozoic cover. In the Cima Lunga unit, ultramafic boudins and lenses form a marker horizon from Alpe Arami, in the south, to Cima di Gagnone in the north (Figure 1). The garnet peridotites of Alpe Arami have attracted a lot of attention in the last 30 years. The origin of this garnet peridotites has been attributed by different studies to: the transition zone, documenting peak pressures of 7–13 GPa and temperatures of 1,100–1,300°C (Dobrzhinetskaya et al., 1996; Green et al., 2010); the hot mantle wedge with peak pressures of 5.9 GPa and 1,180°C (Paquin & Altherr, 2001); or the subducted slab (Trommsdorff et al., 2000) reaching conditions of 3.2 GPa and 840°C (Nimis & Trommsdorff, 2001). All these studies agree that the Alpe Arami peridotites are a slice of mantle that escaped serpentinization and has no evidence for an oceanic setting prior to subduction, such as the presence of associated rodingites. This leaves the possibility open, that the Alpe Arami peridotites have a complex mantle wedge history prior to the incorporation into the subduction channel. Moreover, the metamorphic conditions of coupling between subducted crustal, oceanic units, and the Alpe Arami peridotites are not well constrained. The most promising area to study coupling between felsic, mafic, and ultramafic units is in Cima di Gagnone, where petrological and geochemical data indicate that at least part of these ultramafic lenses were portions of lithospheric mantle exposed to the Piemonte–Liguria ocean floor and serpentinized (Pfiffner & Trommsdorff, 1998; Scambelluri et al., 2014; Trommsdorff et al., 2000).

Geochronological studies on a suite of mafic/ultramafic lenses from the Cima Lunga unit give HP peak metamorphic age of *c*. 35 Ma (Brouwer et al., 2005; Gebauer, 1996; Hermann et al., 2006) and decompression ages of *c*. 32 Ma (Hermann et al., 2006). Considering U–Pb zircon ages obtained in migmatites (Gebauer, 1996; Rubatto et al., 2009) and ages of decompression of garnet peridotite (Hermann

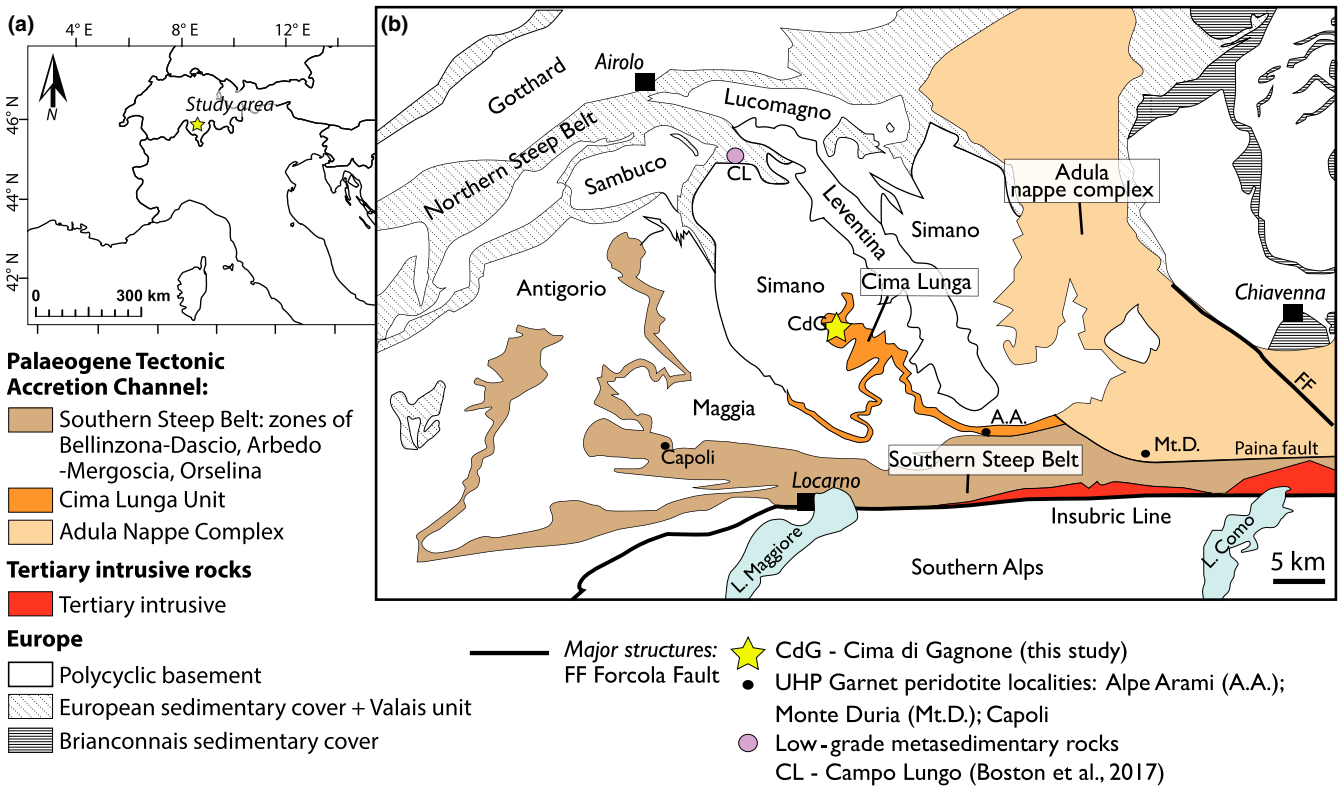

FIGURE 1 (a) Geographic setting of the study area; (b) Tectonic map of the Central Alps and sample location (modified after Berger et al., 2005; Janots et al., 2008; Maxelon & Mancktelow, 2005; Trommsdorff et al., 2000) [Colour figure can be viewed at wileyonlinelibrary.com]

et al., 2006), the exhumation from peak eclogite facies to amphibolite facies conditions must have occurred within 3 Ma (Rubatto et al., 2009). Despite the quite common well-preserved mineral assemblage of the eclogite facies peak in mafic and ultramafic lithologies (2.5–3 GPa; ~800°C), very few metapelitic rocks apparently preserve HP relicts. Previous *P–T* estimates on metapelites from Cima di Gagnone give *P* ranging from 0.6 to 0.7 GPa and temperature ranging from 600 to 650° (Grond et al., 1995; Heinrich, 1982). The whiteschists and sodic whiteschists from the Adula nappe complex still preserve a record of higher pressure, with a peak pressure >2 GPa and temperature ~650°C (Meyre et al., 1999). All these indications of moderate pressures for the metapelitic rocks contrasts with the HP inferred in the mafic, ultramafic lithologies and raise a fundamental question on the mechanisms taking place in the subduction plate interface responsible for the exhumation of this HP unit.

2.1 | Geological background of the study area, Cima di Gagnone

The ultramafic bodies at Cima di Gagnone are composed of lenses of chlorite-harzburgite and garnet peridotite (Evans & Trommsdorff, 1978; Trommsdorff et al., 2000). Peak paragenesis of the chlorite-harzburgite comprises olivine, orthopyroxene, clinopyroxene, chlorite, with accessory Cr-rich magnetite, pentlandite, and pyrrhotite (Pfiffner, 1999; Piccoli et al., 2019; Scambelluri et al., 2014). In garnet peridotite, Cr–Al spinel, Cu sulphide, Fe–Ni–Cu, and Fe–Cu sulphide, pentlandite, Fe–Ni arsenide (+ilmenite, +zircon) are in equilibrium with the peak silicate assemblage composed of olivine, orthopyroxene, and garnet (Pfiffner, 1999; Piccoli et al., 2019; Scambelluri et al., 2015). The discovery of prograde to peak metamorphic amphibole provided further evidence that subduction conditions did not go beyond the amphibole stability field (Pfiffner & Trommsdorff, 1998). Subduction-related peak metamorphic conditions for the ultramafic lenses in Cima di Gagnone have been estimated by phase equilibrium modelling at 750–800°C and ~2.8 GPa (Nimis et al., 1999; Scambelluri et al., 2014).

The enrichment in fluid mobile elements and similarities in the U, Pb, B, Li, and Sr contents of the Cima di Gagnone peridotite with present-day oceanic serpentinites indicate that they represent the dehydration product of subducted abyssal serpentinites. On the basis of this geochemical fingerprint and the occurrence of rodingite dykes, it has been proposed that the ultramafic–mafic-carbonate suite at Cima di Gagnone derived from an ocean basin near a hyperextend continental margin (Pfiffner & Trommsdorff, 1998).

Eclogite facies mafic rocks of Cima di Gagnone are garnet+clinopyroxene metabasalts to metarodingites, with tholeiite geochemical affinity (Evans et al., 1979, 1981). The peak mineral assemblage corresponds to omphacite, garnet, quartz, with minor ilmenite, rutile, epidote, and amphibole. In the outcrops, eclogite lenses show a zonation related to retrograde replacement of the eclogite by plagioclase amphibolites, locally garnet bearing (Cannaò et al., 2015; Heinrich, 1982; Pfiffner & Trommsdorff, 1998). The hydration of the eclogites during retrogression has been associated with the infiltration of H_2O-rich fluids, possibly coming from the enclosing metapelites (Heinrich, 1982).

Isotopic studies of both garnet peridotite (bulk rock Sm–Nd and Lu–Hf in garnet) and eclogites (U–Pb in zircon) yielded Eocene ages of *c*. 40 Ma and 43–35 Ma respectively (Becker, 1993; Brouwer et al., 2005; Gebauer, 1996; Gebauer et al., 1992), consistent with late Eocene HP metamorphism in the Western Alps (Froitzheim et al., 1996; Gebauer et al., 1997; Rubatto et al., 1998).

The metasedimentary rock suite comprises gneiss with pelitic composition and minor amounts of Mesozoic dolomitic marbles and quartzite (Cannaò et al., 2015; Heinrich, 1982; Pfiffner & Trommsdorff, 1998). Relicts of eclogite facies metamorphism in metapelites are restricted to corona and pseudomorph textures (Heinrich, 1982). This latter rock type is the subject of this study.

3 | METHODS

3.1 | Electron probe microanalysis

Mineral chemistry of silicate minerals was determined by wavelength dispersive spectrometer (WDS) using a JEOL JXA 8200 superprobe at the Institute of Geological Sciences of the University of Bern, operating with an acceleration voltage of 15 keV, a probe current of 10 nA, and a beam diameter of 1 μm. Spot analyses were measured for each mineral phase present. The mass fractions of nine element oxides were calibrated using synthetic and natural standards: wollastonite (SiO_2), albite (Na_2O), anorthite (CaO), orthoclase (K_2O), olivine (MgO), anorthite (Al_2O3), tephroite (MnO), almandine–olivine (FeO), and rutile (TiO_2). The investigated thin section was analysed using high-resolution maps acquired using the WDS and point analyses serving as internal standards (Lanari & Piccoli, 2020). Analytical conditions included acceleration voltage of 15 keV and probe current of 100 nA to compensate for the short dwell times (Lanari & Piccoli, 2020). X-ray maps were corrected for dead time, classified, and standardized using XMapTools 2.3 (Lanari et al., 2014, 2019). Structural formulae and maps of end-member proportions were generated using the external functions provided in XMapTools. Spot measurement data are reported in the Appendix S1.

Zircon crystals in thin sections were imaged by charge contrast in low vacuum conditions with a Zeiss EVO50

scanning electron microscope at the University of Bern, working at 15 kV, 100 nA and 10 mm working distance.

3.2 | Laser Ablation-ICP-MS

3.2.1 | Garnet trace element mapping

Major, minor, and trace element maps of garnet were acquired by LA-ICP-MS with a Resonetics RESOlutionSE 193nm excimer laser system equipped with a S-155 large volume constant geometry cell (Laurin Technic, Australia) at the Institute of Geological Sciences, University of Bern, Switzerland. The laser system was coupled with an Agilent 7900 quadrupole ICP-MS instrument. The ICP-MS was tuned for low oxide production (ThO/Th <0.2%) and Th/U ratio close to one (Th/U > 97%). Mapping was performed on a regular 30 µm thick polished thin section. Imaging was achieved by ablating 16 µm large parallel rasters across the sample surface, with a line spacing of 16 µm, and scan speed of 22 µm/s (Maps in Figure 7a) or 10 µm/s (Map in Figure 7b). Pre-ablation of each raster was performed for minimizing the effect of re-deposition. Ablation was performed in an atmosphere of pure He (0.7 L/min) and N_2 (0.003 L/min) mixed with Ar (0.86 L/min) immediately after the ablation cell. A laser repetition rate of 10 Hz and fluence on sample of 7 J/cm^2 were employed (compare Raimondo et al., 2017 for analytical conditions). Data acquisition was performed in time-resolved analysis mode as a single continuous experiment. Background (60 s) and primary standard GSD-1g were analysed every 15 min, secondary standard SRM-NIST 612 every 30 min. Each analysis comprised a series of 29 elements for a total sweep time of 0.411 s (see Table S2.1 in the Appendix S2).

Data reduction was performed using the software *Iolite* (Hellstrom et al., 2008; Paton et al., 2011; Woodhead et al., 2007). Instrument drift and mass bias were corrected for applying a linear fit between the data set of standards; background was also subtracted from each raster. Quantification was performed using ^{27}Al for internal calibration based on weighted average of EPMA wt% Al_2O_3. As this calibration is only valid for garnet, only garnet compositions are shown and discussed in the following.

Data from Iolite were imported into XMapTools and further processed using the chemical modules and sampling tools (Lanari & Piccoli, 2020).

3.2.2 | Zirconium in Rutile

Zirconium in rutile measurement by LA-ICP-MS was performed at the Institute of Geological Sciences, University of Bern (see above for the details on the instrument). A laser repetition rate of 5 Hz and fluence on sample of 3 J/cm^2 were employed. Data acquisition was performed in time-resolved analysis mode. Background (60 s), primary standards SRM-NIST610, and secondary standards GSD-1g were measured at the beginning and end of the sequence. Each analysis comprised a suite of 14 element masses for a total sweep time of 0.24 s (Table S2.3 in the Appendix S2). Quantification was performed using ^{49}Ti for internal calibration assuming 99 wt% TiO_2.

3.3 | Phase equilibrium modelling

Phase diagrams were calculated using the software Perple_X (version 6.8.7, Connolly, 2009) and the internally consistent thermodynamic database of Holland and Powell (1998, revised 2004). Mineral solid solution models (Fuhrman & Lindsley, 1988; Green et al., 2007; Holland & Powell, 1996, 1998; Tajčmanová et al., 2009; White et al., 2001) were used for omphacite (Omph(GHP)), garnet (Gt(HP)), phengite (Pheng(HP)), biotite (Bio(TCC)), plagioclase (Pl(h)), and melt (melt(HP)). Rutile and ilmenite were considered as pure phases. Phase diagrams were calculated for the system Na–K–Mn–Ti–CaFMASH (assuming H_2O and SiO_2 as saturated components, see Table S2), using local bulk composition determined by combining the mineral modes, mineral compositions, and compositional maps and density correction to derive weight fractions (Lanari & Engi, 2017). Allanite pixels were excluded while calculating the reactive bulk composition and therefore in the model it is assumed that allanite was not part of the reactive volume of this rock at HP. Since there is no significant Fe^{3+} component in the other phases, we decided to restrict the model to a simple ferrous system. The model of Ti-bearing phengite Mica(CHA1) of (Auzanneau et al., 2010) was also tested (Figure S1). Phase relations at peak do not differ much from that obtained with the Pheng(HP) model, but Mica(CHA1) cannot reproduce the measured Ti content in phengite. We therefore use the experimental curve of Hermann and Spandler (2008) separately to estimate the *P–T* conditions of the phengite core composition (first generation of phengite).

4 | RESULTS

4.1 | Petrographic observations

The sample investigated in this study is a two mica, kyanite, garnet bearing metapelite found adjacent to the garnet peridotite lens in Cima di Gagnone (Figure 1; outcrop MG160 in Pfiffner & Trommsdorff, 1998). The main schistosity is formed by the grain-shape preferred orientation of mica (28 vol.%) and kyanite (~2 vol.%), anastomosing around relics of large white mica flakes and garnet (Figure 2).

Garnet (14 vol.%) displays two main textures: subhedral and atoll shaped/resorbed. Observed inclusions in garnet

are: quartz, white mica, zircon, and rutile (Figure 3a,b,e; Figure S2). No coesite or radial cracks around quartz inclusions in garnet were observed. In addition, quartz is found only as an inclusion in garnet, but it is absent in the mineral matrix. Resorbed garnet grains also display rutile lamellae in both mantle and rim (Figure 3f). Euhedral zircons are found in inclusion in garnet and in the mineral matrix. In both microstructural positions, zircon grains are relatively small (20–50 μm long, Figure 4) and display CL-bright cores with oscillatory zoning, surrounded by an unzoned CL-dark rim (Figure 4). No sigmoidal lines of inclusions (i.e. snowball structure) in garnet are observed, and crystals are wrapped around by the schistosity. This suggests that garnet crystallization is prekinematic (Figure 5).

Large white mica flakes are found as randomly oriented inclusion in subhedral and atoll-shaped garnet, suggesting that the two minerals crystallized at the same time (Figures 2a, 3b, 5). In the mineral matrix, white micas are aligned along the schistosity, wrapping around garnet and large white mica flakes (Figures 2a and 3). Therefore, white mica is here interpreted as pre- to synkinematic.

Kyanite occurs as prismatic/partially resorbed crystals aligned along the schistosity planes, often overgrown by biotite (Figure 3c).

Resorbed epidote crystals (<1 vol.%) are found within the schistosity planes. Some of the crystals display an allanitic core of few tens of microns, recognizable in crossed-polarized light and well visible in backscattered electron images.

Rutile is found as inclusion in garnet and in the mineral matrix along the schistosity planes. Rutile in the matrix is consistently surrounded by an ilmenite rim (Figure 3c), suggesting that rutile remained stable until amphibolite facies overprint (Figure 5).

Brown biotite (25 vol.%) occurs as post-kinematic crystals cutting across the schistosity and replacing white mica flakes. Large biotite flakes are also observed within atoll-shaped garnet (Figure 3a).

Plagioclase is the main component of the mineral matrix with a volume abundance of 30 vol.%. Plagioclase crystals are randomly oriented, statically replacing the pre- synkinematic assemblage, and are optically zoned (Figures 3d and 5).

4.2 | Mineral chemistry

Garnet displays significant differences in major element composition at the scale of the thin section (Figure 2). Three compositional domains can be recognized (Figures 2b and 6b): (a) domain D1 is characterized by garnet grains with highest pyrope and grossular content (X_{Prp} of 0.3, X_{Grs} 0.2); (b) domain D2 has garnet with X_{Prp} ranging from 0.24 to 0.25, with rare outer rim with lower X_{Prp} ranging between 0.16 and 0.21; (c) a narrow domain D3 located between D1 and D2 is characterized by garnet with the lowest pyrope content (X_{Prp} of ~0.2) and lowest grossular content (X_{Grs} ~0.13). Low Mg grains (X_{Prp} of 0.2) display higher Mn and Ca. Minor internal zoning in Ca (X_{Grs}) ranging between 0.12 and 0.15, is observed in almost every grain (Figure 7d), whereas garnet are not zone in Mg, Fe, and Mn.

Microstructural observations indicate that white mica are pre- to synkinematic. Chemical analyses provide evidence for a more complex white mica growth and three different generations are distinguished on the basis of their chemistry. This is particularly evident when plotting mapped mica Si versus Ti concentrations. The microprobe map pixel density distribution shows that there are three different populations with distinct Si–Ti contents (Figure 6a). Pre-kinematic, large

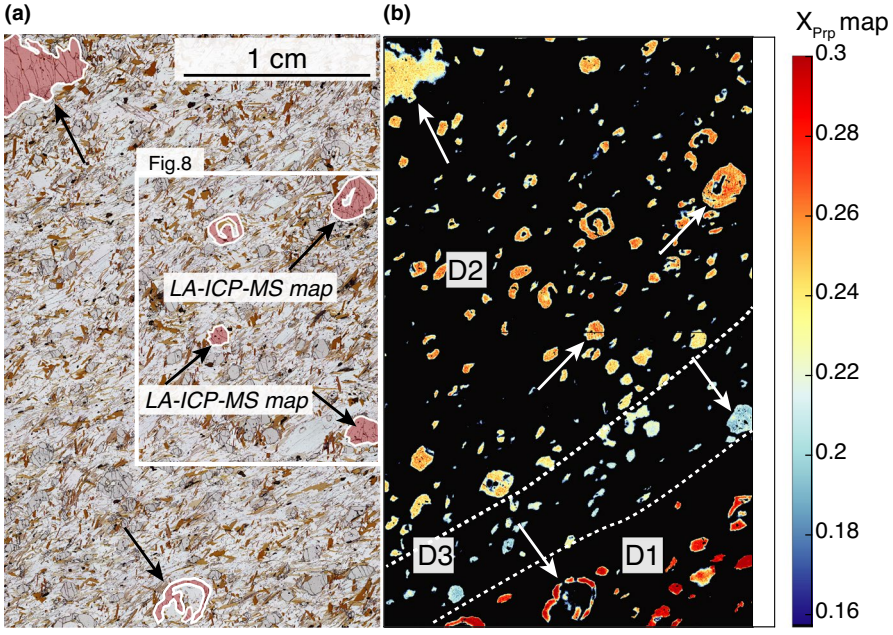

FIGURE 2 (a) Thin section scan showing the presence of garnet with subhedral, atoll-shaped/resorption texture indicated by black arrows. (b) X-ray map of the thin section showing the variation in Mg content of garnet expressed as percentage of X_{Prp}. White arrows indicated subhedral, resorbed/atoll-shaped garnet and mapped garnet as indicated in (a) [Colour figure can be viewed at wileyonlinelibrary.com]

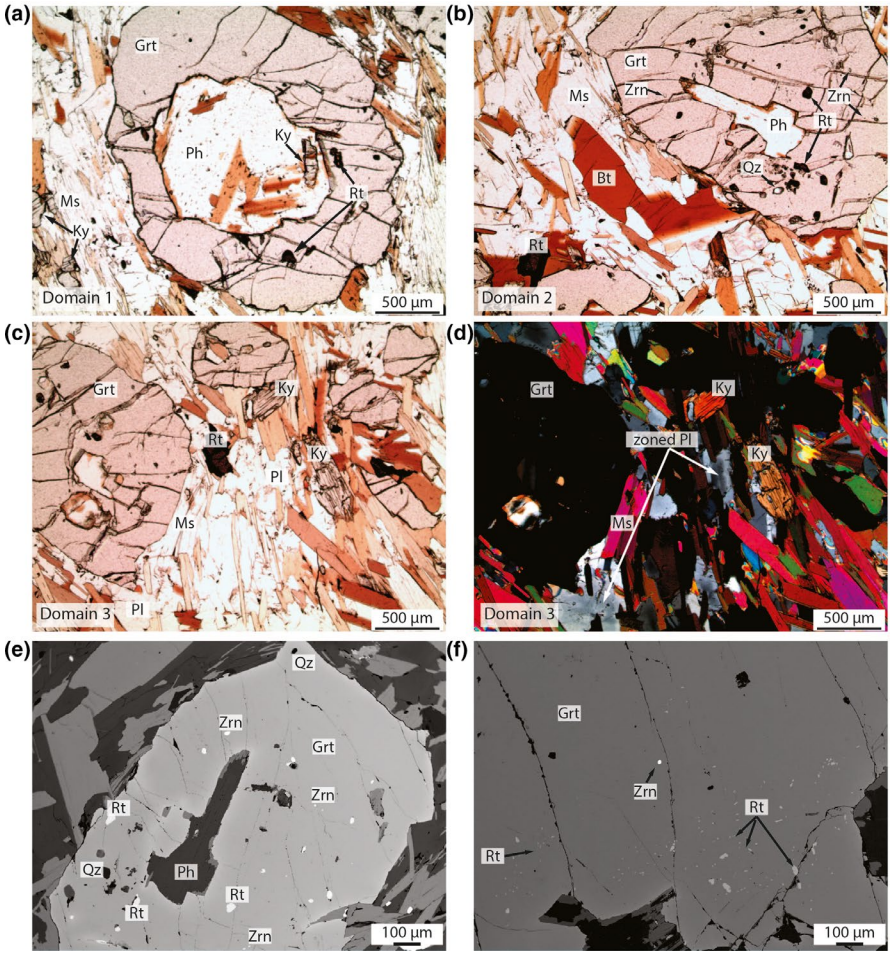

FIGURE 3 Thin section photomicrographs. (a) Atoll-shaped garnet from Domain 1 with rutile inclusions (plane polarized light). (b) Subhedral garnet from Domain 2 with phengite, rutile, zircons (+quartz) inclusions (plane polarized light). (c) White mica wrapping around garnet crystals from Domain 3 and post-kinematic biotite (plane-polarized light). (d) Cross-polarized light of (c) showing zoned plagioclase in the matrix. (e) Backscattered electron image of garnet from Domain 2 (see also b) with quartz, rutile and zircon inclusions. (f) Rim of resorbed garnet from Domain 2 with inclusions of rutile crystals and small rutile lamellae [Colour figure can be viewed at wileyonlinelibrary.com]

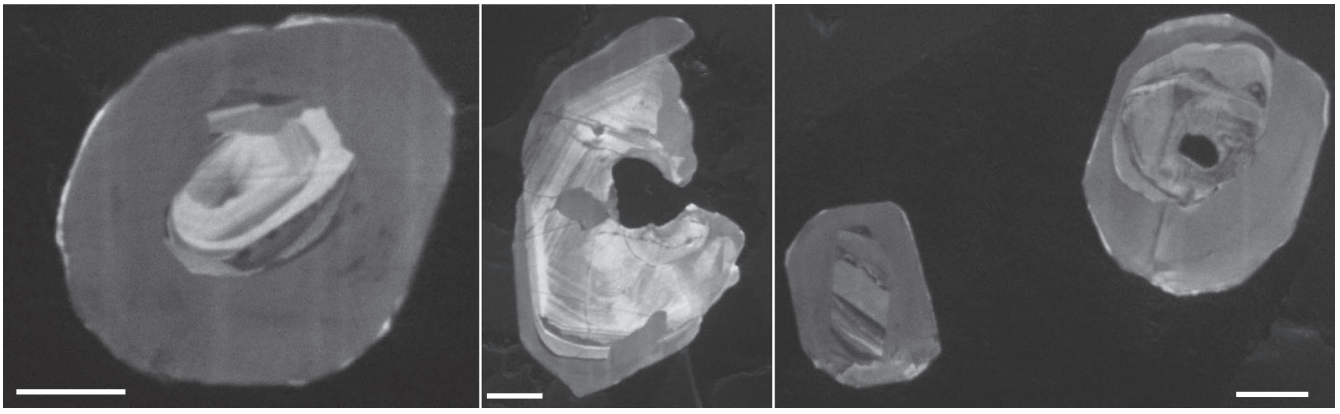

FIGURE 4 Charge contrast images of zircons showing a magmatic core with oscillatory zoning and unzoned metamorphic rim. Scale bar is 20 µm

phengite flakes in inclusion in garnet and in the mineral matrix are strongly zoned in Ti and Si (Figure 7a,b). Cores always have a high TiO_2 content, up to 1.5 wt%, and Si of ~3.25 atoms per formula unit (a.p.f.u.). Rims have lower TiO_2 (<0.8 wt%) and higher Si (3.34 a.p.f.u.). Most of the synkinematic, small crystals in the matrix are zoned, with a phengite core with high Si and low Ti, and a muscovite rim, with low TiO_2 (<0.5 wt%) and low Si (~3 a.p.f.u.) (Figure 7a,b).

All measured feldspars are Na–Ca plagioclase and display sharp core–rim zoning, with decreasing albite and increasing anorthite content (X_{Ab} passing from 80% to 50% from core to rim, Figures 5 and 7c).

Brown biotite crystals are chemically homogenous and have an intermediate composition between annite and phlogopite (X_{Eas} 0.17, $X_{siderophyllite}$ 0.17, X_{Phl} 0.26, X_{Ann} 0.26, and $X_{Ti\text{-}biotite}$ 0.14), with homogenous X_{Mg} and no Ti zonation (Appendix S1).

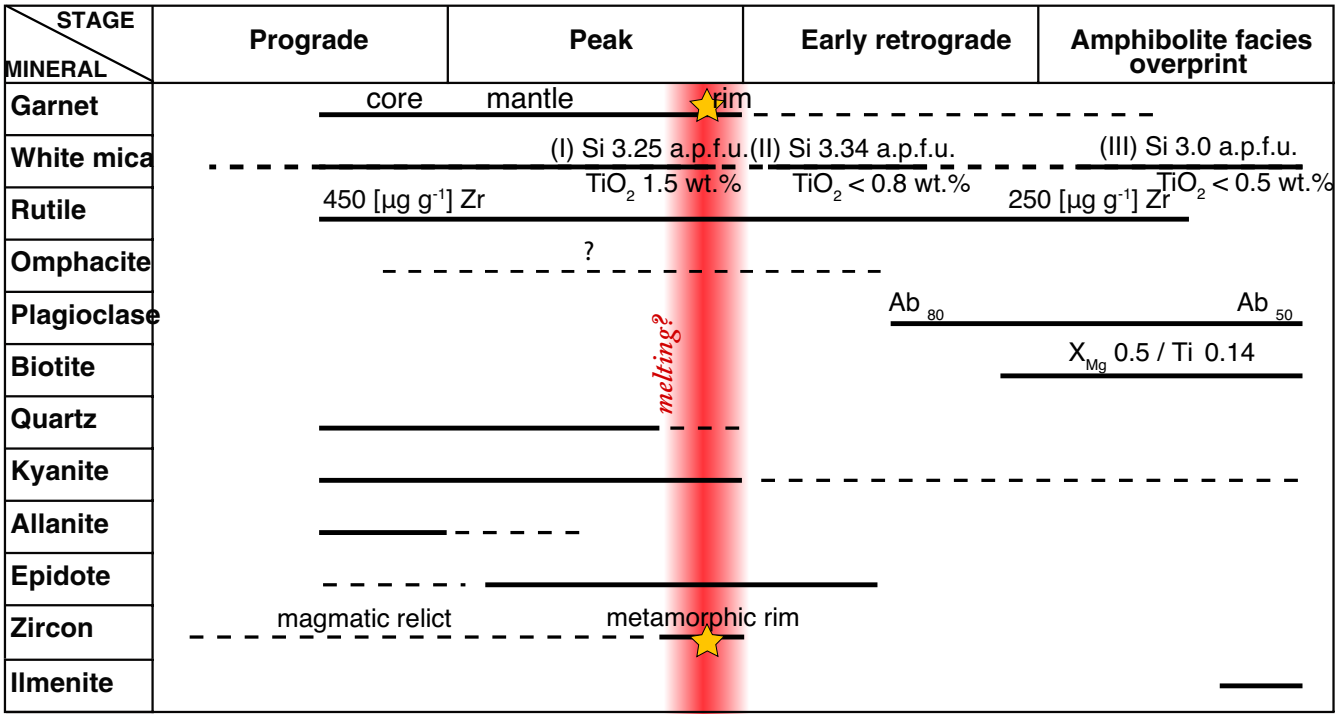

FIGURE 5 Petrogenetic table reporting the main petrographic observations and mineral chemistry information used to reconstruct the metamorphic history. The metamorphic evolution is subdivided in four stages: prograde, peak, early retrograde, and amphibolite facies overprint. The stars indicate that the evidence for partial melting is found in garnet and zircon [Colour figure can be viewed at wileyonlinelibrary.com]

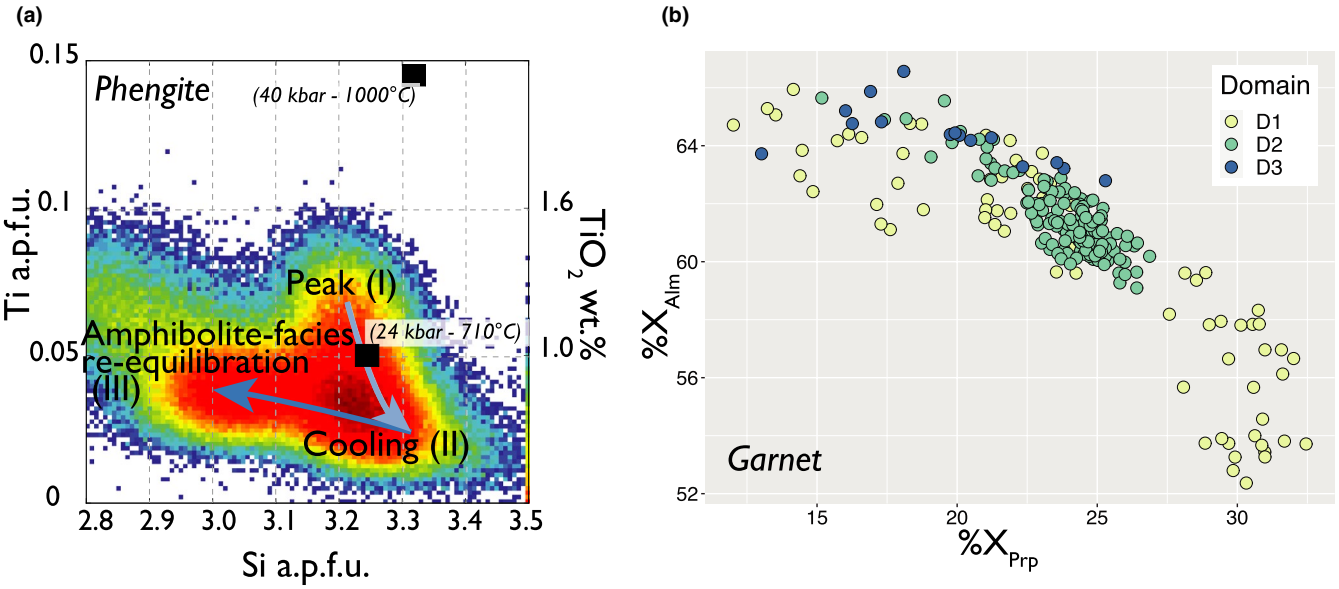

FIGURE 6 (a) White mica Si a.p.f.u. versus Ti a.p.f.u. and weight per cent plot showing the three generation of white mica (see also Figure 7a,b). The plot was generated with density function based on white mica compositions. Black squares are phengite composition from the UHP Kokchetav complex (Stepanov, Hermann, et al., 2016). The significance of the arrows is discussed in text; (b) Garnet X_{Alm} versus X_{Prp} plot [Colour figure can be viewed at wileyonlinelibrary.com]

4.3 | Garnet trace element composition

Spot analyses and three quantitative maps were performed on different garnet grains selected for their petrographic texture (i.e. atoll shaped, subhedral, Figure 3), microstructural position (D1, D2, D3; Figure 2b), and major element composition (e.g. X_{Prp}, Figure 2b). Figure 8 reports maps of middle and heavy rare earth elements (HREEs) for each of the three mapped garnet from D2 to D3, together with the respective chondrite-normalized REE plot. Figure 9 shows

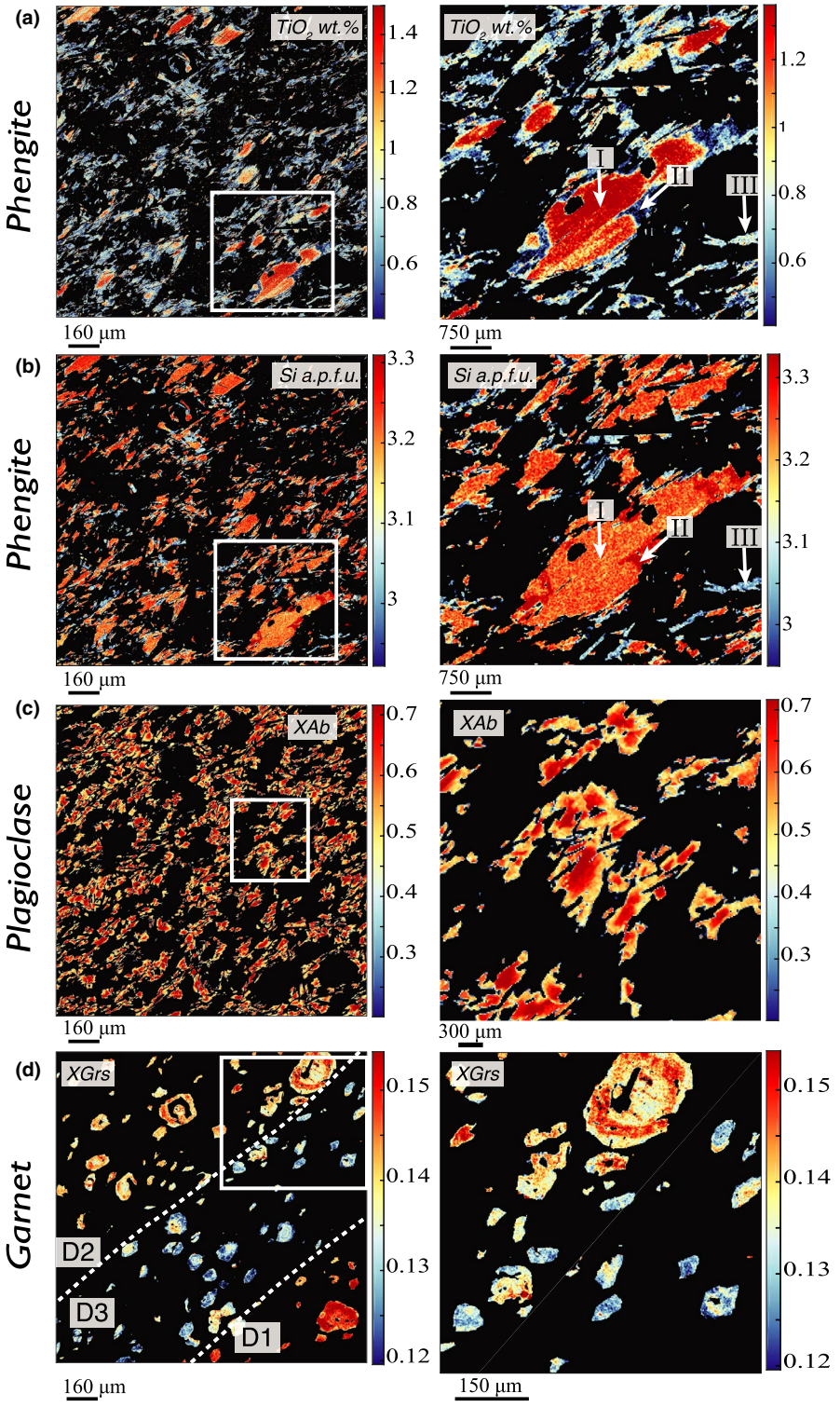

FIGURE 7 Representative compositional maps of phengite (a and b), plagioclase (X_{Ab}=albite/albite+anorthite) (c), and garnet (d) [Colour figure can be viewed at wileyonlinelibrary.com]

chondrite-normalized REE patterns for spot analyses (14 individual grains, Table S2.2 in the Appendix S2).

Different garnet generations were recognized on the basis of HREE zoning, which suggests a classic prograde trend of decreasing concentration from the first to the second generation (Figures 8 and 9). Noteworthy, the last garnet generation displays HREE enrichment (Figures 8 and 9). Based on trace element patterns, different garnet generations were then classified as core (first generation), mantle (second generation), and rim (last generation) (Figure 8). All garnet measured by both spot analysis and mapping have a slightly negative Eu anomaly of 0.65 ($Eu_N/Eu^* = E_N \Big/ (\sqrt[2]{Sm_N \times Gd_N})$), likely inherited from the pelitic protolith (Cannaò et al., 2015), suggesting that they

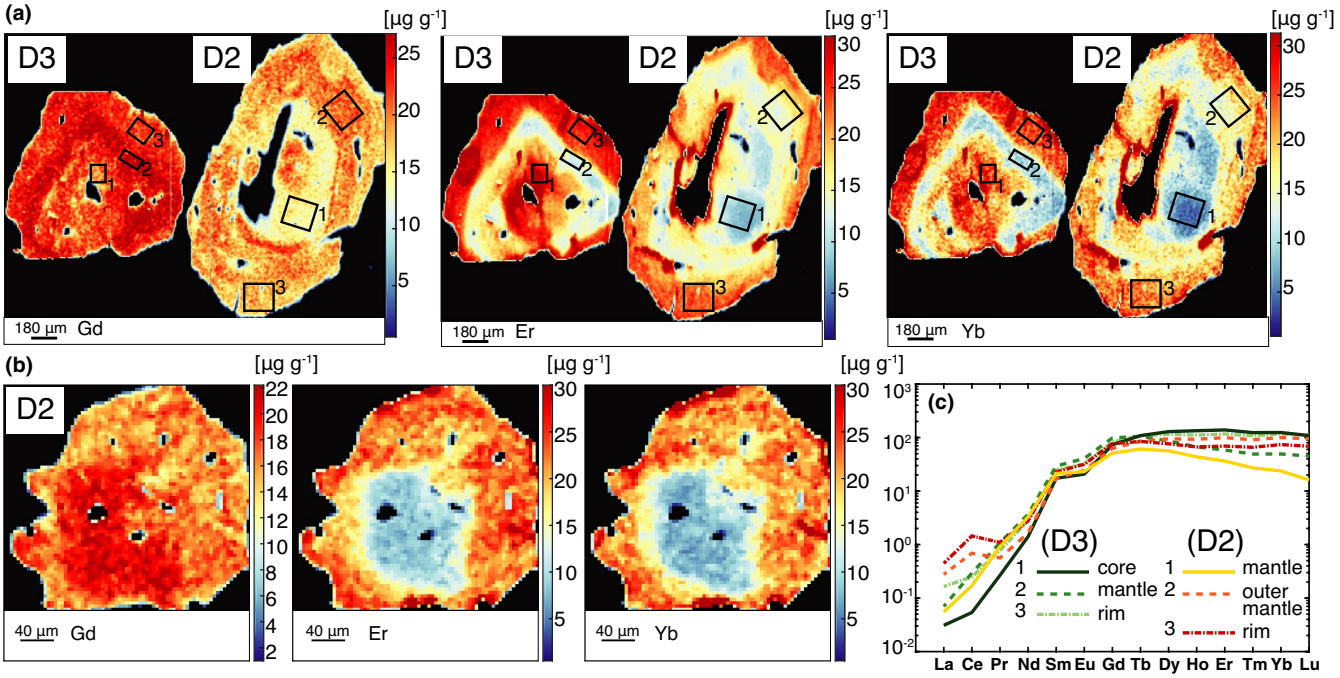

FIGURE 8 Garnet maps and Chondrite-normalized REE patterns. (a) Domain 2 and Domain 3 garnet zoning. Black boxes represent the pixel sampling area to extract composition displayed in (c). (b) Garnet from Domain 2 displaying similar zoning to garnet in (a). (c) Chondrite-normalized REE patterns for different domains of garnet in (a) [Colour figure can be viewed at wileyonlinelibrary.com]

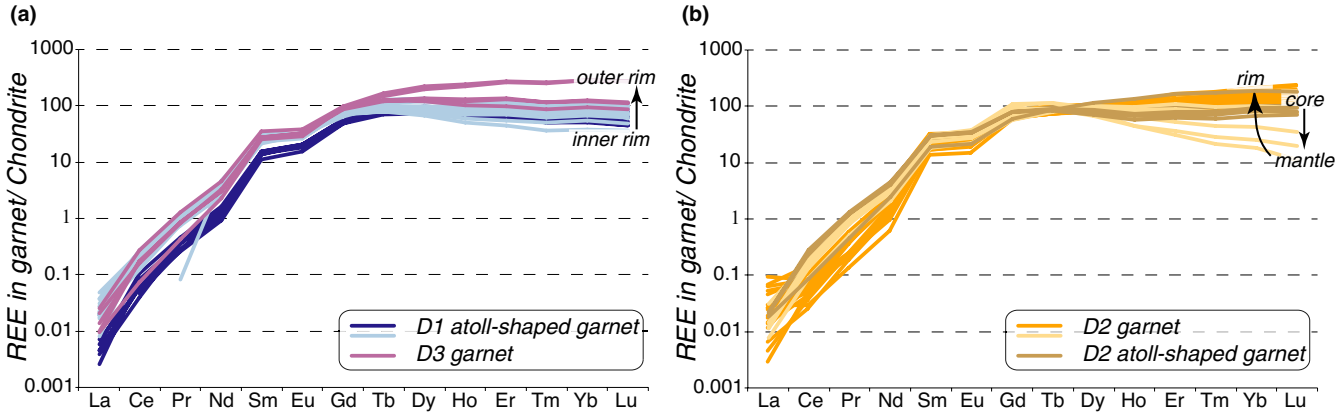

FIGURE 9 Chondrite-normalized REE patterns of garnet from D1 and D3 (a) and D2 (b) [Colour figure can be viewed at wileyonlinelibrary.com]

grew in a plagioclase-absent environment. The Eu anomaly is much less pronounced than what would be expected from a garnet growing in equilibrium with plagioclase (Ague, 2017).

Subhedral garnet have a HP content in the mantle (up to 300 $\mu g/g$, Figure 10a). The evolution of P displays a positive correlation with Zr (Figure 10b). Highest P and Zr concentrations are observed in garnet from D1 to D2, in particular in core and mantle domains (Figure 10a). Outer garnet rims, atoll-shaped garnet and garnet from D3 display the lowest concentration (Figure 10b).

4.4 | Zirconium in rutile

Rutile is found preserved as inclusions in garnet and in the matrix (Figure 3). In total, 14 individual grains were analysed by LA-ICP-MS (Table S2.4 in the Appendix S2). Silicon, ^{90}Zr, ^{91}Zr, and Fe were monitored during measurement in order to avoid zircon and ilmenite contaminations. Spot size ranged from 16 to 38 μm, depending on grain size. Overall, the rutile inclusions in garnet have high Zr (up to 450 μg/g median value of 404 μg/g Figure 11), with the exception of grains in inclusion in the atoll-shaped garnet from Z1 (lowest

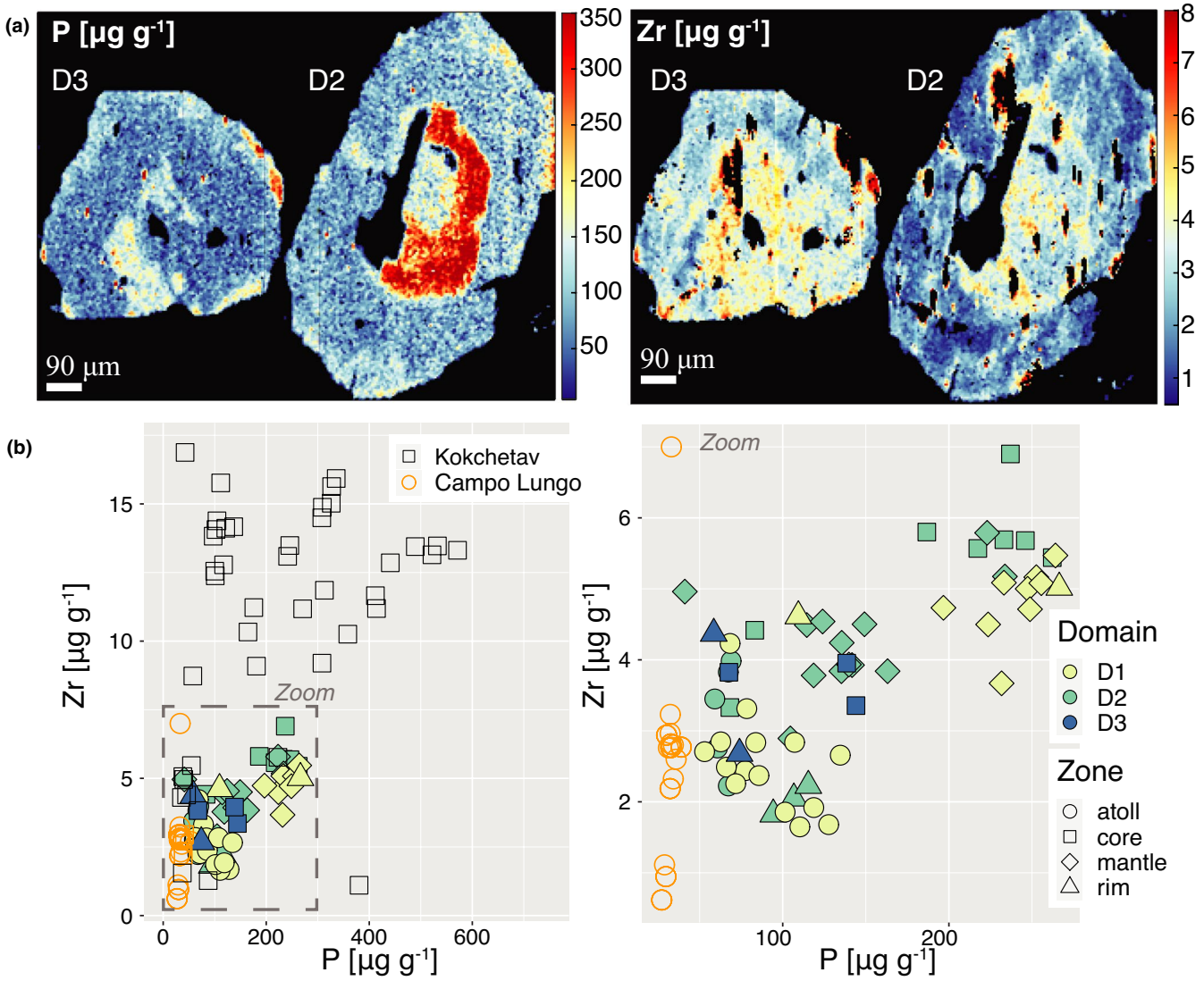

FIGURE 10 (a) Phosphorous and Zirconium LA-ICP-MS maps in garnet from D3 and D2. (b) Phosphorous versus Zirconium concentration in garnet. Garnet composition from the *LP–LT* unit of Campo Lungo, Central Alps (Boston et al., 2017) and from Barchi-Kol *UHP* terrain, Kokchetav Complex (Stepanov, Hermann, et al., 2016) are reported for comparison [Colour figure can be viewed at wileyonlinelibrary.com]

value in Figure 11). Rutile in the matrix displays significantly lower Zr (median value of 248 μg/g, Figure 11).

4.5 | Thermodynamic modelling

Two isochemical phase diagrams in the Na_2O–K_2O–MnO–TiO_2–CaO–FeO–MgO–Al_2O_3–SiO_2–H_2O system were calculated to explore the effects of variable local bulk compositions on garnet composition (D1 and D2), especially in MgO (Figure 12a,b respectively; Table S3). Figure 12 displays the phase diagrams for the two reactive bulk compositions, calculated assuming H_2O and SiO_2 saturation. Modelled HP and low-*P* (LP) assemblages are identical in both diagrams. High X_{Prp} (~0.3) in garnet and high Si in phengite (3.34–3.36 a.p.f.u.) are predicted and match the measured compositions at 700–750°C and 2.5 GPa for D2 (Figure 12b). For the same *P–T* conditions, the model applied to D1 predicts garnet with X_{Prp} >0.32. The intersection between second phengite generation and garnet isopleths supports formation at HP–HT conditions (purple dot in Figure 12b). Omphacite is predicted to be stable at these conditions; however, fresh omphacite was not identified as inclusions in garnet or in the matrix. Note that most of the garnet cores are resorbed, hence inclusions of omphacite and/or coesite were probably lost. Nevertheless, plagioclase displays a sharp zoning with a high albite core and a high anorthite rim, suggesting that a Na-rich pyroxene omphacite+quartz might have been converted to plagioclase during decompression. A complete retrogression of omphacite into plagioclase upon exhumation is also supported by the modelled mode of omphacite (~20 vol.%) and observed mode of plagioclase (~30 vol.%).

Kyanite is stable in both HP and LP fields. The modes of kyanite modelled at HP (800° and 2.7 GPa) and LP (1.0 GPa and 620°C) are 1.5 and 0.5 vol.% respectively. In this sample,

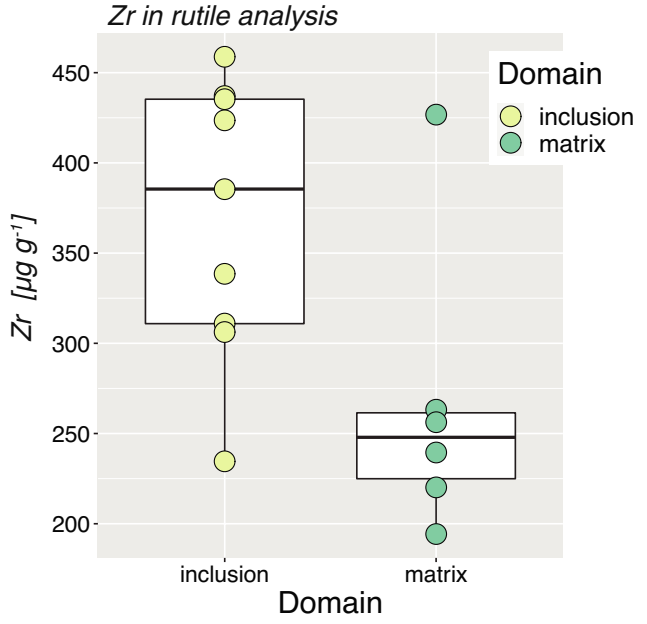

FIGURE 11 Zirconium concentration in rutile classified by microstructural position (inclusion in garnet, yellow dots; grain in the matrix, green dots). Measurements of rutile in the matrix yield a median value of Zr content of 248 ppm, median Zr concentration in rutile in inclusion in garnet is 385 ppm [Colour figure can be viewed at wileyonlinelibrary.com]

~2 vol.% of kyanite is assessed from the phase map (Table S3). The modelled kyanite abundance fits the observation at higher pressure conditions of 2.9 GPa. This observation suggests that kyanite might have grown during peak eclogite facies conditions and was partially resorbed during exhumation.

Garnet resorption and mineral chemistry suggest a significant degree of re-equilibration during decompression by dissolution–precipitation and net transfer reactions. This latter interpretation is supported by the modelled mineral modes. Garnet modal proportion passes from ~30 vol.% at HP to ~15 vol.% at LP. Figure 12c shows the volume proportion isopleths for garnet, phengite, and plagioclase. A good match between observed and modelled modes is found at 1.0 GPa and ~620°C (blue dot in Figure 12c). These *P–T* conditions are in line with previous estimates of the amphibolite facies metamorphic stage (Boston et al., 2017; Grond et al., 1995; Heinrich, 1982), even though the pressure is 0.3–0.4 GPa higher than previously reported (Heinrich, 1982; Lanari & Hermann, 2020).

5 | DISCUSSION

5.1 | Reconstructing the *P–T* evolution of metapelites from Cima Lunga Unit

The reconstruction of the metamorphic history of HP and UHP terranes is often challenging because of high degrees of re-equilibration, manifested for example by disequilibrium texture (e.g. resorption) and retrograde reactions, such as biotite and plagioclase formation. Therefore, *P–T* determination hinges on the investigation of key metamorphic minerals that might preserve several pieces of the earliest rock's metamorphic history (Figure 5).

Here we attempt to reconstruct the *P–T* path of the metapelite associated with garnet peridotite at Cima di Gagnone, with a focus on rutile, phengite, and garnet texture and major and trace element geochemistry, aided by thermodynamic simulations. Petrological and geochemical data provided in this work show that micaschists associated with an ultramafic lens at Cima di Gagnone underwent a prograde *P–T* path from HP–MT to HP–HT metamorphic peak (Figure 13).

5.1.1 | Zirconium in rutile thermometry

The first constraint for the prograde path is the Zr in rutile thermometer (Tomkins et al., 2007). A systematic difference is found between rutile grains included in garnet showing high Zr content versus rutile grains in the matrix showing low Zr content (Figure 11). Experimental constraints on the diffusion rate of trace elements in rutile, such as Zr, suggest that diffusive re-equilibration should reset rutile composition during cooling on a scale of micrometre to tens of micrometres over a range of temperature from 600 to 800°C (Cherniak et al., 2007; Marschall et al., 2013). If the metasediments reached only a MT metamorphic peak conditions (e.g. ~620°C), similar Zr concentrations are expected in rutile grains from both microstructural positions. On the contrary, if the rock underwent metamorphic temperature as high as 800°C as indicated by Ti in phengite, (see Section 5.1.2) and, possibly, partial melting, Zr-in-rutile from the matrix could have diffused much faster and re-equilibrated during the amphibolite facies stage. Amphibolite facies re-equilibration is also suggested by the good match of 200 µg/g Zr in rutile isopleth and estimated *P–T* conditions for the amphibolite facies stage (Figure 12c). Therefore, only rutile inclusions in garnet, which have higher Zr content than the matrix grains, are representative of prograde crystallization temperatures. Rutile was entrapped in garnet at eclogite facies ($P > 2.0$ GPa). At this pressure, Zr concentration indicates temperature of ~725–750°C (Figure 12b, Tomkins et al., 2007). This temperature is below that obtained from the Ti in phengite thermobarometry (see Section 5.1.2), but higher than the temperature reported in previous studies for peak pressure amphibolite facies metamorphism (Boston et al., 2017; Todd & Engi, 1997). We interpret the obtained temperature of ~725–750°C as representative for crystallization conditions during prograde eclogite facies metamorphism (green dot in Figure 12c).

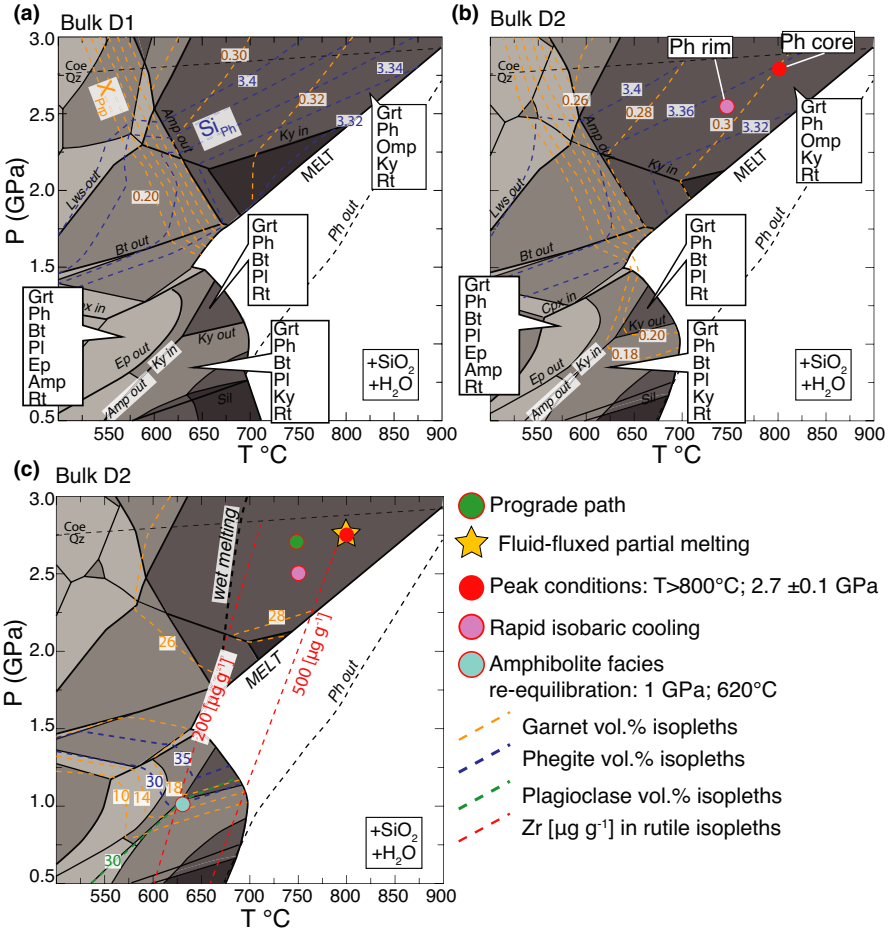

FIGURE 12 *P–T* phase diagram together with X_{Prp} isopleths (dashed orange lines) and Si in phengite isopleths (dashed blue lines) for bulk D1 (a) and bulk D2 (b). (c) Phase diagram reporting prograde, peak, and retrograde conditions. Zirconium-in-rutile isopleths are from Tomkins et al. (2007). Wet melting curve from Hermann and Spandler (2008). Grt = garnet solid solution, Omp = omphacite solid solution, Lws = lawsonite, Amp = amphibole, Ky = kyanite, Bt = biotite solid solution, Ph = phengite solid solution, Cpx = clinopyroxene solid solution, Ep = epidote solid solution, Rt = rutile, Sill = sillimanite, Coe = coesite, Qz = quartz [Colour figure can be viewed at wileyonlinelibrary.com]

5.1.2 | Phengite thermobarometry

Silicon and Ti contents in phengite are a powerful indicator of the *P–T* conditions of eclogite facies metapelites at (U) HP (Lang & Gilotti, 2007; Stepanov et al., 2016). Also in our case study, phengite shows compositional zoning in Si and Ti. Experimental data on phase relations in subducted pelites can be used to evaluate simultaneously the effects of pressure and temperature on the Si and Ti contents in phengite (Auzanneau et al., 2010; Hermann & Spandler, 2008) for an assemblage of phengite, garnet, kyanite, clinopyroxene, rutile, and coesite/quartz that is equivalent to the observed paragenesis. The experimental calibration curve of Hermann and Spandler (2008) was used to determine *P–T* conditions of the large phengite flake core (population (I) in Figure 6a). Based on these experimental data, with a TiO_2 content of 1.5 wt% (Figure 7a) and Si of 3.25 a.p.f.u. (Figure 7b), the phengite flake core formed at temperature >800°C and pressure >2.5 GPa. Using garnet isopleths in the calculated pseudosection, pressure can be constrained to between 2.6 and 2.75 GPa, that is just below the quartz–coesite transition at 800°C (red dot in Figure 12b,c). These conditions are significantly higher than previously estimated for the Cima Lunga metasedimentary unit (pressure at eclogite facies, temperature unconstrained, Cannaò et al., 2015; Heinrich, 1982).

Thermodynamic models can be used to constrain the second generation of phengite, which has a slightly higher Si and lower Ti content. Reproducing this second-generation phengite composition by thermodynamic simulation is crucial to understanding the early stage of exhumation (purple dot in Figure 12b,c). The high Si content (3.34 a.p.f.u.) and low Ti (TiO_2 <0.8 wt%) suggest that peak metamorphic conditions were followed by near-isobaric cooling (Figures 6a and 12b,c). This is supported by thermodynamic modelling that predicts the stability of high Si phengite with high X_{Prp} garnet at pressure of ~2.5–2.6 GPa and temperature ~700–750°C (Figure 12b).

5.1.3 | Garnet composition: Evidence for HP–HT metamorphism

In rocks that underwent HT metamorphism, distinguishing garnet chemical domains (i.e. core–mantle–rim) using major elements can lead to significant bias due to different extents of diffusion and/or re-equilibration. An alternative approach is to recognize the different chemical

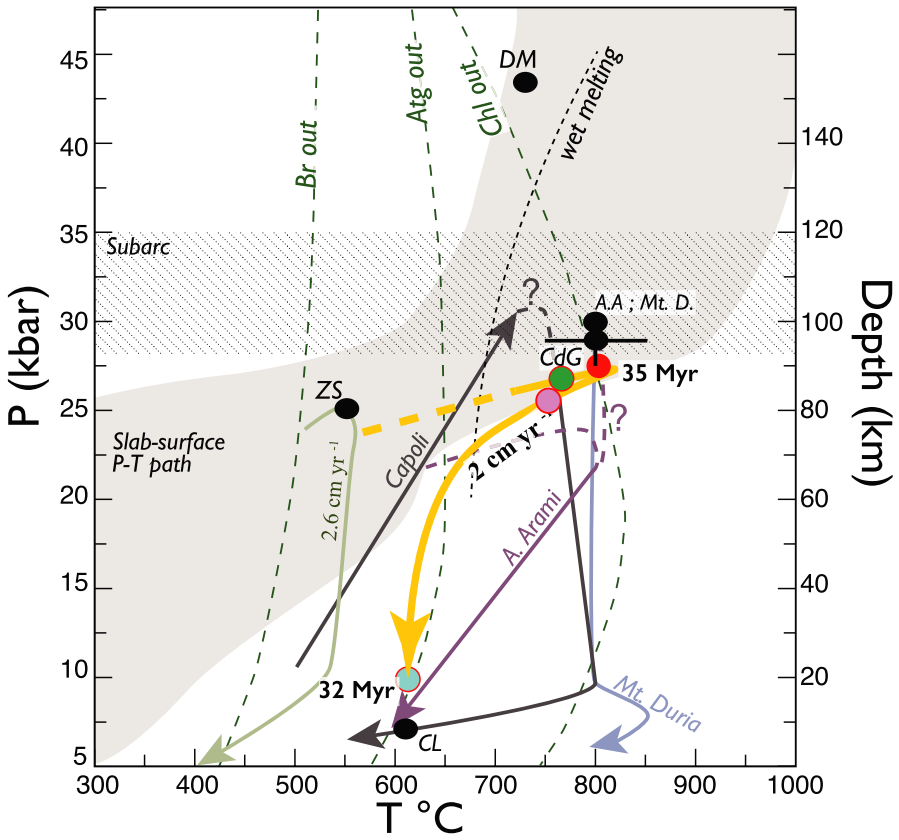

FIGURE 13 *P–T* paths for the study metapelite (yellow arrow) and for Zermatt-Saas ophiolitic unit (ZS; Amato et al., 1999; Angiboust et al., 2009), eclogite (dashed line), and ultramafic rocks (solid line indicates common path) from Alpe Arami and Capoli (Brouwer et al., 2005; Nimis et al., 1999), and from Mt. Duria (Hermann et al., 2006; Tumiati et al., 2018). Note that in both literature cases the early exhumation path of ultramafic rocks is not constrained. Peak metamorphic conditions for garnet bearing white schists from Dora Maira (DM; Hermann, 2003) and metasediments from Campo Lungo (CL; Boston et al., 2017) are also reported. Slab surface *P–T* path (grey band) from Syracuse et al. (2010). Cima di Gagnone error bars for *P–T* estimations in ultramafic lithologies (CdG) are from Scambelluri et al. (2014). Metamorphic ages are for Alpe Arami, Mt. Duria (Brouwer et al., 2005; Gebauer, 1996; Hermann et al., 2006) [Colour figure can be viewed at wileyonlinelibrary.com]

domains based on the interpretation of trace element patterns (Rubatto et al., 2020). REE patterns of analysed garnet are characteristic of crystallization at eclogite facies where plagioclase is no longer stable (Figures 8 and 9). This is supported by the observation of an identical Eu/Eu* anomaly in garnet core and mantle (this study) and in bulk rock composition (Cannaò et al., 2015). Another indication of a HT event is the positive trend between P and Zr content (Figure 10b). Figure 10b reports data for the low-grade metapelites from Campo Lungo, which have the same mineralogical assemblage of this study rock (Boston et al., 2017) and UHP–UHT metapelite from the Kokchetav complex (Stepanov, Rubatto, et al., 2016). It can be seen that garnet from Cima di Gagnone metapelite have a clearly different composition compared to the low-grade garnet from Campo Lungo (orange open circles in Figure 10b) and form a trend of increasing P–Zr, indicating crystallization at high temperature and higher pressure conditions, from core to mantle. Atoll-shaped garnet, which was more prominently re-equilibrated during the retrograde path, displays lower Zr, but still high P compared to the low-grade metapelites from Campo Lungo.

Although garnet trace element patterns suggest a common metamorphic evolution of crystallization at eclogite facies, major element compositions display more complexities, such as different compositional domains at the scale of the thin section (Figure 2). This spatial distribution can be explained by two main mechanisms that are not mutually exclusive. The first mechanism is diffusion in a fluid-absent system. This process requires the presence of pre-existing compositional domains, such as sedimentary layers. Locally different bulk rock compositions controlled garnet re-homogenization of major elements by diffusion, imposing a chemical potential gradient between the interior and the inter-granular medium, but this mechanism is sluggish in the absence of fluid (Carlson, 2010). Theoretical calculation and experimental studies predict that Fe and Mg diffuse at the same speed at elevated pressure and temperature (Carlson, 2006; Chakraborty & Ganguly, 1992; Chu & Ague, 2015) and they diffuse significantly faster than Ca

(Chu & Ague, 2015). This is consistent with the measured Ca zoning in garnet from D2 and the homogenous Mg–Fe content. Even if elevated temperature favoured diffusion at the grain scale, chemical gradients were preserved at the scale of the thin section (Figure 2). The chemical potential of MgO, μ_{MgO}, at 800°C and 2.7 GPa is −631.7 kJ/mol in D1 and −632.3 kJ/mol in D2, resulting in a difference of 0.6 kJ/mol. If initial compositional domains were present, chemical potential gradients would have been flattened by diffusion at HT. It was proposed based on numerical simulations that grain scale stress variations can smooth chemical potential gradients and slow down/terminate diffusion (Tajčmanová et al., 2014, 2015). However, as far as we are aware, this process has never been documented in experimental or field-based studies.

The second mechanism is diffusion and new growth of peritectic garnet in the presence of melt. This mechanism requires garnet re-equilibration by intragranular diffusion near peak, which is likely at these HT conditions, and new growth of peritectic garnet. Different degrees of melt extraction from different domains, and thus different re-equilibration between post-peak and amphibolite facies conditions, can potentially explain the formation of the compositional domains observed in thin section.

5.1.4 | Amphibolite facies re-equilibration

Extensive re-equilibration during amphibolite facies metamorphism is documented by the presence of minerals, such as biotite and plagioclase, by resorption texture in garnet (e.g. embayed rims, atoll-shaped garnet, Figures 2 and 3; Giuntoli et al., 2018; Robyr et al., 2014), and by multiple white mica generations. In particular, the last white mica generation, muscovite, characterized by low Si (3 a.p.f.u.) and low Ti (TiO_2 <1 wt%) is related to LP partial re-equilibration after the eclogite facies peak. Kyanite is predicted to be stable both at HP and LP (Figure 12). The modal abundance (determined by XMapTool image analysis) matches best the model at HP (2.75 GPa) and is higher than the one predicted at LP. Kyanite may have been partially resorbed upon amphibolite facies overprint. In addition, neither andalusite nor sillimanite were observed in our sample. This observation is consistent with modelled peak pressure amphibolite facies metamorphic conditions of ~620°C and 1.0 GPa, inferred by mineral assemblage and mineral abundance (light blue dot in Figure 12c), which is also consistent with field evidence that no late Alpine migmatites are observed in metapelites at Cima di Gagnone. Our estimate for the amphibolite facies stage is in agreement with previous studies in the region (Boston et al., 2017; Grond et al., 1995; Heinrich, 1982; Meyre et al., 1999; Todd & Engi, 1997).

5.2 | Evidence and implications for a common *P–T* path of mafic, ultramafic, and metapelitic rocks from Cima di Gagnone

5.2.1 | Comparing *P–T* estimates for mafic eclogites, garnet peridotites, and metapelites

Much literature exists on the petrology and geochemistry of ultramafic and mafic rocks from the Cima Lunga unit. Mafic eclogites are locally overprinted by Oligocene amphibolite facies metamorphism (Evans et al., 1979; Heinrich, 1986). Investigation of preserved eclogite cores in amphibolite boudins gave estimations for the peak metamorphic conditions at 800°C and ~2.5 GPa. *P–T* estimates for ultramafic lithologies yielded similar eclogitic peak pressure conditions of ~3 GPa, and temperature for garnet peridotite of 740–800°C (Nimis et al., 1999; Scambelluri et al., 2014). All these indications for elevated pressure and temperature recorded in mafic and ultramafic lithologies contrast with moderate pressures and temperatures deduced from the mineralogy of pelitic rocks in previous work (Irouschek, 1980; Meyre et al., 1999; Wenk, 1955). It was proposed that this contrast may be explained by different overprinting rates, where the dehydrating metapelite was re-equilibrating faster than dry mafic, ultramafic lenses (Heinrich, 1982). The presence of coronitic textures (Heinrich, 1982) was interpreted as an indication that the eclogitic assemblage phengite+garnet was replaced by amphibolite facies muscovite+biotite+feldspar, although the author did not estimate the peak *P–T* conditions. Our data show that peak metamorphic conditions of metapelite from Cima di Gagnone are, within uncertainty, identical to those of ultramafic and mafic rocks (Figure 13). Therefore, despite the presence of mechanically heterogeneous rocks, we found no supporting evidence for significant pressure deviations above lithostatic (overpressure), which might be expected at the outcrop scale if transient high differential stress occurs (Chu et al., 2017; Luisier et al., 2019; Schenker et al., 2015).

Estimated amphibolite facies conditions (~620°C and 1.0 GPa) are in line with the presence of talc in the ultramafic rocks together with tremolite and cummingtonite, indicating amphibolite facies overprint (Evans & Trommsdorff, 1974; Pfiffner, 1999; Rice et al., 1974; Scambelluri et al., 2014). Altogether, our *P–T* path reconstruction (Figure 13) shows that metapelite and ultramafic rocks were very likely coupled at least since prograde/near peak eclogitic conditions and also shared a common exhumation path. The finding of a common metamorphic history for the ultramafic, mafic, and metapelitic rocks simplifies the geodynamic scenario of burial and exhumation the Cima di Gagnone HP metamorphic suite (see Section 5.3.1) and provides support to chemical and isotopic data that point to chemical exchange between ultramafic and metasedimentary rocks during prograde to peak metamorphic conditions (Cannaò et al., 2015; Scambelluri et al., 2014).

5.2.2 | Dehydration in ultramafic rocks and fluid-fluxed melting of associated metapelites

No clear field evidence such as the presence of leucosomes exists in the investigated area that is characteristic of partial melting, as also observed by another recent study in the same area (Corvò et al., 2021). However, the calculated bulk major element composition of the investigated sample contains only 45 wt% SiO_2 and high Al_2O_3 (25 wt%), suggesting that the investigated sample likely represents a residuum. Bulk rock REE patterns with negative slope (Cannaò et al., 2015), are consistent with partial melting at ~800°, where bulk LREE depletion in the residue is not expected because accessory phases (e.g. allanite) are not completely exhausted (Hermann & Rubatto, 2009). For such a residual bulk composition, melting is not predicted by thermodynamic calculations at peak conditions. Microstructural evidence for the former presence of melt can be modified and/or erased during the melting event as well as during the subsequent deformation history of the rock (Holness et al., 2011). In the absence of direct textural evidence the most robust information about potential HP melting is recorded in refractory phases such as garnet and zircon (Stepanov, Rubatto, et al., 2016). The most convincing evidence would be the preservation of melt inclusions in garnet (Stepanov et al., 2016) or in zircon (Cesare et al., 2003; Kawakami et al., 2013; Rubatto et al., 2009) but no melt inclusion has been observed. Nevertheless, all garnet (from all domains) display an enrichment in HREE at the outer rim (Figure 8). Such an enrichment could be explained by resorption or new growth during partial melting. The sharp zoning, the extent of the HREE-rich domain, and the constant compositions all support the hypothesis of new garnet growth during partial melting. In the presence of melt, accessory phases such as apatite, monazite, and zircons partially dissolve and P, Zr, and HREE are incorporated in such peritectic garnet (Rubatto et al., 2020). Neither apatite nor monazite were observed in thin section. Consumption of apatite and partial consumption of clinozoisite might explain the observation of Ca-rich garnet (Figure 7d). Such Ca enrichment in garnet during melting at UHP conditions has been reported in studies from other metamorphic terranes (Lang & Gilotti, 2007, 2015; Perchuk et al., 2005). Melting is also supported by the formation of metamorphic zircon rims (Figure 4). Similar growth of metamorphic rims over relict magmatic cores is reported in migmatites from the Southern Steep Belt (Figure 1), where melting occurred due to aqueous fluid infiltration (Rubatto et al., 2009), but it has never been observed in zircon from lower amphibolite facies metapelites (e.g. Campo Lungo, Figure 1; Boston et al., 2017). Preliminary results of U–Pb dating in zircon rims from similar samples reported by Corvò et al. (2021) suggest that zircon rims from a sample adjacent to an ultramafic lens indeed crystallized during an early Alpine metamorphism at *c*. 36 Ma that would be consistent with the age of HP metamorphism (Gebauer et al., 1992). Lastly, the occurrence of abundant post-kinematic biotite around and within atoll-shaped garnet (Figure 3) suggests that biotite formed as retrograde reaction of hydrous melt and garnet (Holness et al., 2011). Therefore, we speculate that the fluid liberated during the transition from chlorite- to garnet peridotite triggered fluxed melting in the associated metapelites. It is worth noting that at Cima di Gagnone, most of the ultramafic lenses (chlorite peridotites) are not fully dehydrated. The rather limited amount of fluid might explain the scarce and only local field evidence for melting. A more detailed study on zircon ages and possible melt inclusions in garnet and zircon is needed to further support this hypothesis.

5.2.3 | Possible interaction of felsic melts with ultramafic rocks

Previous studies investigated geochemical indicators for fluid-mediated interaction between ultramafic and felsic rocks at Cima di Gagnone. The lack of extensive phlogopite veins or other geochemical fingerprints in the ultramafic rocks for infiltration of migmatite derived fluids, such as strong enrichment in LILE, suggests that the felsic melt did not interact with ultramafic rocks (Scambelluri et al., 2014). Previous works interpreted the bulk rock Be enrichment and the relatively high $^{87}Sr/^{86}Sr$ (0.709–0.7124) of ultramafic rocks as a consequence of exchange with the host micaschists during subduction (Cannaò et al., 2015; Scambelluri et al., 2014). An alternative process that could explain the elevated $^{87}Sr/^{86}Sr$ signature is crust–mantle interaction upon exhumation of subcontinental mantle below a hyper-extended continental margin, by infiltration of low-*T* seawater bearing suspended detrital particulates (e.g. Harvey et al., 2014; Hattori & Guillot, 2007; Salters & Stracke, 2004; Snow et al., 1993). We therefore suggest that during subduction, the main direction of aqueous fluid flow was coming from the dehydrating serpentinized mantle towards the associated metasediments. Later fluid-mediated interaction likely happened during exhumation as indicated by Pb isotopes systematics (Cannaò et al., 2015).

5.3 | Implications for the geodynamic reconstruction of the Central Alps

5.3.1 | Structural position versus metamorphic history: A comparison to the Adula nappe and the Bellinzona Dascio zone

Field structural studies pointed out that the Cima Lunga unit is not the equivalent of the Adula nappe to the East because,

compared to other gneissic units, mafic and ultramafic bodies are more abundant (Schenker et al., 2015, 2019). There is a clear distinction between the central part of the Adula nappe complex (Trescolmen area), which underwent HP–MT metamorphism of ~650°C and 2.4 GPa (Meyre & Puschnig, 1993), and the Cima Lunga unit (~800°C and ~3 GPa), although they are now situated at a comparable structural position within the Alpine nappe stack. Most recent studies agree that garnet peridotite lenses from the Cima Lunga unit reached a maximum Alpine HP metamorphic peak of ~3 GPa, (Nimis & Trommsdorff, 2001; Scambelluri et al., 2014). Estimation of peak metamorphic conditions of the garnet peridotites from the southern part of the Cima Lunga unit (Alpe Arami) has been subject of controversy with pressures ranging from 3 to 17 GPa (Becker, 1993; Dobrzhinetskaya et al., 1996; Evans & Trommsdorff, 1978; Green et al., 2010; Nimis & Trommsdorff, 2001; Nimis et al., 1999; Paquin & Altherr, 2001). There is the possibility that these peridotites have a complex metamorphic history in the mantle wedge prior to the incorporation into the subducted slab. We suggest that the main equilibration stage of the garnet peridotites at 3.2 GPa and 840°C (Nimis & Trommsdorff, 2001) likely represents the conditions when the Arami peridotites were incorporated into the Alpine subduction channel.

Comparable metamorphic conditions to that of Cima di Gagnone and Alpe Arami were observed in ultramafic rocks from the southern part of the Adula nappe (i.e. Monte Duria peridotite, ~800–850°C—~3 GPa, Hermann et al., 2006; Nimis et al., 1999), and ultramafic rocks from the Western Bellinzona-Dascio zone (i.e. Capoli, Southern Steep Belt, Brouwer et al., 2005). Evidence for HP metamorphism was also found in felsic lithologies from the southern Adula nappe by the investigation of trace element composition in metamorphic zircons (Liati et al., 2009). These authors could not conclude if peak metamorphic temperature exceeded 800°C. The absence of massive melting in the gneisses can be explained if the rocks remained mostly anhydrous, because melting is not expected to occur at temperature below 950°C (Hermann & Green, 2001; Spandler et al., 2010). Peak metamorphic conditions of mafic, ultramafic, and metapelitic rocks of Cima di Gagnone are close to that of the southernmost part of Adula nappe (Monte Duria) and the ultramafic lens of Capoli in the Southern Steep Belt, opening up the possibility that the Cima Lunga unit may have been subducted and exhumed as a coherent metamorphic unit.

5.3.2 | Slab heating, break-off, and exhumation

Microstructural and geochemical features such as preservation of fossil chemical gradients in garnet and different phengite generations indicate that the studied metapelite underwent HT metamorphism (800°C, 2.7 GPa), followed by rapid, near-isobaric, cooling (700–750°C, purple dot in Figure 12). Isobaric cooling is followed by decompression to lower pressure and temperature of 1.0 GPa and 620°C corresponding to the amphibolite facies overprint (Figure 12). A rapid exhumation of 2 cm/year is proposed based on geochronological data available in literature for HP peak (35 Ma) and amphibolite facies stage (32 Ma) of ultramafic lenses in the Adula and Cima Lunga unit (Boston et al., 2017; Brouwer et al., 2005; Gebauer, 1996; Hermann et al., 2006). This *P–T–t* path contrasts with those reported for other UHP ultramafic lenses from the Adula Nappe, the Cima Lunga unit and the Bellinzona-Dascio zone (Monte Duria, Alpe Arami, Capoli), for which it is proposed that near isothermal decompression took place prior to cooling after amphibolite facies overprint (Figure 13; Brouwer et al., 2005; Hermann et al., 2006; Nimis et al., 1999; Tumiati et al., 2018). Also in the Western Alps, for the eclogite facies Zermatt Saas unit, it is proposed a rapid isothermal exhumation after peak (Figure 13; Amato et al., 1999; Angiboust et al., 2009). To our knowledge, this study is the first report of near-isobaric cooling in rocks that underwent HP–HT metamorphism from the Central Alps.

Two possible geodynamic scenarios can be outlined to explain the observed peak conditions at HP–HT. The favoured scenario for this study is that the ultramafic-metasedimentary suite of Cima di Gagnone is a fossil ocean–continent transition (Pfiffner & Trommsdorff, 1998; Trommsdorff et al., 2000); hence, it was in a favourable position for reaching near UHP condition (~3 GPa) following the down pulling force of the negatively buoyant oceanic lithosphere (Beltrando et al., 2010, 2014). Exhumation of very dense garnet peridotites was then enabled by the presence of inherited structures, such as oceanic faults, that worked as preferred detachment surfaces (Beltrando et al., 2014; Lundin & Doré, 2011; Mohn et al., 2011) and/or because associated, partially melted, metasediments acted as a positive buoyancy force. Exhumation can also be favoured by slab extraction as suggested for the Adula nappe by Froitzheim et al., (2003). Alternatively, rapid exhumation rate and the presence of partially melted metapelites are also consistent with a model of exhumation based on Stokes flow where the UHP garnet peridotite are embedded in low viscosity and high density partially melted metapelites.

In all cases, the slab break-off might have favoured the exhumation (Figure 14a). Several studies constrain the Central Alps slab break-off at 35 Ma and ~100 km depth (von Blanckenburg & Davies, 1995; Kästle et al., 2020; Kissling & Schlunegger, 2018). The proximity of the Cima Lunga unit to the slab window would explain the observed heating followed by almost isobaric cooling (Figure 13). A strong thermal gradient would be imposed from the flow of asthenospheric mantle into the slab window (Figure 14b) and the

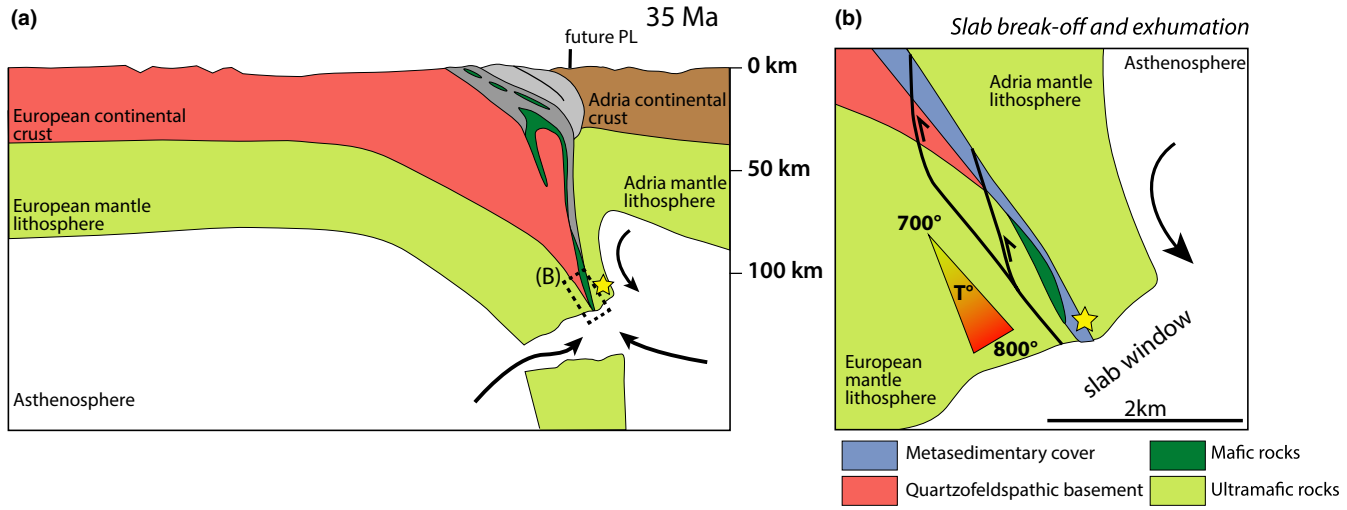

FIGURE 14 (a) Geodynamic sketch of the European–Adria convergent margin at 35 Ma. (b) Sketch of the starting of the exhumation because of slab break-off. Close to the slab window, a strong temperature gradient exists. With exhumation, a small difference in pressure corresponds to a large difference in temperature [Colour figure can be viewed at wileyonlinelibrary.com]

starting of the exhumation would result in a drop of temperature and only slight decrease in pressure, consistent with the mineral record (Figure 12c). Slab break-off and consequent fast cooling/exhumation is consistent with the presented petrological and geochemical features.

6 | CONCLUSIONS

The detailed textural and petrological–geochemical study of metapelites associated with HP garnet peridotite from Cima di Gagnone reveals multiple metamorphic stages, from peak HP–HT conditions (2.7 ± 0.1 GPa and 800°C) to retrograde (amphibolite facies) conditions (1.0 GPa and 620°C). Microprobe and LA-ICP-MS mapping distinguishes different growth zones in phengite and garnet, and provides evidence for fluid-assisted melting during subduction. A detailed, previously unreported, prograde-–peak and early retrograde *P–T* path was reconstructed. Importantly, peak conditions closely match those of the associated ultramafic lenses (Figure 13). Fast, near-isobaric cooling after peak conditions is inferred and suggests that exhumation was initiated by slab break-off (Figure 14). Wet melting of metapelites might also have favoured this process, acting as buoyant force and weakening the rock unit thus favouring fast exhumation/cooling.

Lastly, we speculate that metapelites and ultramafic rocks were coupled before subduction or at least in its early stage. This finding opens new scenarios for the geodynamic interpretation of the Cima Lunga unit. We propose that the ultramafic lenses at Cima di Gagnone were parts of the exhumed and serpentinized mantle emplaced at the hyper-extended European continental margin. Slices of the margin were detached during slab break-off and tectonically mixed in the subduction channel.

ACKNOWLEDGEMENTS

This work was supported by the Swiss National Science Foundation grants No. 200021_172688 to T.P., 200021_169062 to J.H, and 206021_170722 to D. Rubatto and T.P. Bernardo Cesare is thanked for editorial handling and for his constructive comments. Jane Gilotti and Jaroslaw Majka are thanked for their thorough and constructive review of this work. Daniela Rubatto is thanked for the assistance with zircon charge contrast imaging and interpretation.

CONFLICT OF INTEREST

The authors declare that there are no competing interests.

ORCID

Francesca Piccoli https://orcid.org/0000-0001-9941-0103
Pierre Lanari https://orcid.org/0000-0001-8303-0771
Jörg Hermann https://orcid.org/0000-0001-8360-3592
Thomas Pettke https://orcid.org/0000-0002-5784-0639

REFERENCES

Agard, P., Yamato, P., Jolivet, L., & Burov, E. (2009). Exhumation of oceanic blueschists and eclogites in subduction zones: Timing and mechanisms. *Earth-Science Reviews*, *92*(1–2), 53–79. https://doi.org/10.1016/j.earscirev.2008.11.002

Ague, J. J. (2017). Element mobility during regional metamorphism in crustal and subduction zone environments with a focus on the rare earth elements (REE). *American Mineralogist*, *102*(9), 1796–1821. https://doi.org/10.2138/am-2017-6130

Amato, J. M., Johnson, C. M., Baumgartner, L. P., & Beard, B. L. (1999). Rapid exhumation of the Zermatt-Saas ophiolite deduced from high-precision Sm-Nd and Rb-Sr geochronology. *Earth and Planetary Science Letters*, *171*(3), 425–438. https://doi.org/10.1016/S0012-821X(99)00161-2

Angiboust, S., Agard, P., Jolivet, L., & Beyssac, O. (2009). The Zermatt-Saas ophiolite: The largest (60-km wide) and deepest (c. 70–80 km) continuous slice of oceanic lithosphere detached from a subduction zone? *Terra Nova*, *21*(3), 171–180.

Auzanneau, E., Schmidt, M., Vielzeuf, D., & Connolly, J. D. (2010). Titanium in phengite: A geobarometer for high temperature eclogites. *Contributions to Mineralogy and Petrology*, *159*(1), 1. https://doi.org/10.1007/s00410-009-0412-7

Becker, H. (1993). Garnet peridotite and eclogite Sm-Nd mineral ages from the Lepontine dome (Swiss Alps): New evidence for Eocene high-pressure metamorphism in the central Alps. *Geology*, *21*(7), 599–602. https://doi.org/10.1130/0091-7613(1993)021<0599:GPAESN>2.3.CO;2

Beltrando, M., Compagnoni, R., & Lombardo, B. (2010). (Ultra-) high-pressure metamorphism and orogenesis: An Alpine perspective. *Gondwana Research*, *18*(1), 147–166. https://doi.org/10.1016/j.gr.2010.01.009

Beltrando, M., Manatschal, G., Mohn, G., Dal Piaz, G. V., Brovarone, V., Alberto, A., & Masini, E. (2014). Recognizing remnants of magma-poor rifted margins in high-pressure orogenic belts: The Alpine case study. *Earth-Science Reviews*, *131*, 88–115. https://doi.org/10.1016/j.earscirev.2014.01.001

Berger, A., Mercolli, I., & Engi, M. (2005). The central Lepontine Alps: Notes accompanying the tectonic and petrographic map sheet Sopra Ceneri (1: 100'000). *Schweizerische Mineralogische Und Petrographische Mitteilungen*, *85*(2–3), 109–146.

Boston, K. R., Rubatto, D., Hermann, J., Engi, M., & Amelin, Y. (2017). Geochronology of accessory allanite and monazite in the Barrovian metamorphic sequence of the Central Alps, Switzerland. *Lithos*, *286*, 502–518. https://doi.org/10.1016/j.lithos.2017.06.025

Brouwer, F., Burri, T., Engi, M., & Berger, A. (2005). Eclogite relics in the Central Alps: PT-evolution, Lu-Hf ages, and implications for formation of tectonic mélange zones. *Schweizerische Mineralogische Und Petrographische Mitteilungen*, *85*(2–3), 147–174.

Burov, E., Jolivet, L., Le Pourhiet, L., & Poliakov, A. (2001). A thermomechanical model of exhumation of high pressure (HP) and ultra-high pressure (UHP) metamorphic rocks in Alpine-type collision belts. *Tectonophysics*, *342*(1–2), 113–136. https://doi.org/10.1016/S0040-1951(01)00158-5

Cannaò, E., Agostini, S., Scambelluri, M., Tonarini, S., & Godard, M. (2015). B, Sr and Pb isotope geochemistry of high-pressure Alpine metaperidotites monitors fluid-mediated element recycling during serpentinite dehydration in subduction mélange (Cima di Gagnone, Swiss Central Alps). *Geochimica et Cosmochimica Acta*, *163*, 80–100. https://doi.org/10.1016/j.gca.2015.04.024

Carlson, W. D. (2006). Rates of Fe, Mg, Mn, and Ca diffusion in garnet. *American Mineralogist*, *91*(1), 1–11. https://doi.org/10.2138/am.2006.2043

Carlson, W. D. (2010). Dependence of reaction kinetics on H_2O activity as inferred from rates of intergranular diffusion of aluminum: Reaction kinetics and aluminium diffusion. *Journal of Metamorphic Geology*, *28*(7), 735–752. https://doi.org/10.1111/j.1525-1314.2010.00886.x

Carry, N., Gueydan, F., Brun, J.-P., & Marquer, D. (2009). Mechanical decoupling of high-pressure crustal units during continental subduction. *Earth and Planetary Science Letters*, *278*(1–2), 13–25. https://doi.org/10.1016/j.epsl.2008.11.019

Cavargna-Sani, M., Epard, J.-L., & Steck, A. (2014). Structure, geometry and kinematics of the northern Adula nappe (Central Alps). *Swiss Journal of Geosciences*, *107*(2–3), 135–156. https://doi.org/10.1007/s00015-014-0175-7

Cesare, B., Gomez-Pugnaire, M. T., & Rubatto, D. (2003). Residence time of S-type anatectic magmas beneath the Neogene Volcanic Province of SE Spain: A zircon and monazite SHRIMP study. *Contributions to Mineralogy and Petrology*, *146*(1), 28–43. https://doi.org/10.1007/s00410-003-0490-x

Chakraborty, S., & Ganguly, J. (1992). Cation diffusion in aluminosilicate garnets: Experimental determination in spessartine-almandine diffusion couples, evaluation of effective binary diffusion coefficients, and applications. *Contributions to Mineralogy and Petrology*, *111*(1), 74–86. https://doi.org/10.1007/BF00296579

Chemenda, A. I., Mattauer, M., Malavieille, J., & Bokun, A. N. (1995). A mechanism for syn-collisional rock exhumation and associated normal faulting: Results from physical modelling. *Earth and Planetary Science Letters*, *132*(1–4), 225–232. https://doi.org/10.1016/0012-821X(95)00042-B

Cherniak, D., Manchester, J., & Watson, E. (2007). Zr and Hf diffusion in rutile. *Earth and Planetary Science Letters*, *261*(1–2), 267–279. https://doi.org/10.1016/j.epsl.2007.06.027

Chu, X., & Ague, J. J. (2015). Analysis of experimental data on divalent cation diffusion kinetics in aluminosilicate garnets with application to timescales of peak Barrovian metamorphism, Scotland. *Contributions to Mineralogy and Petrology*, *170*(2), 25. https://doi.org/10.1007/s00410-015-1175-y

Chu, X., Ague, J. J., Podladchikov, Y. Y., & Tian, M. (2017). Ultrafast eclogite formation via melting-induced overpressure. *Earth and Planetary Science Letters*, *479*, 1–17. https://doi.org/10.1016/j.epsl.2017.09.007

Connolly, J. (2009). The geodynamic equation of state: What and how. *Geochemistry, Geophysics, Geosystems*, *10*(10). https://doi.org/10.1029/2009GC002540

Corvò, S., Maino, M., Langone, A., Schenker, F. L., Piazolo, S., Casini, L., & Seno, S. (2021). Local variations of metamorphic record from compositionally heterogeneous rocks (Cima di Gagnone, Central Alps): Inferences on exhumation processes of (U)HP–HT rocks. *Lithos*, *390-391*, 106126. https://doi.org/10.1016/j.lithos.2021.106126

Dale, J., & Holland, T. (2003). Geothermobarometry, P-T paths and metamorphic field gradients of high-pressure rocks from the Adula Nappe, Central Alps. *Journal of Metamorphic Geology*, *21*(8), 813–829. https://doi.org/10.1046/j.1525-1314.2003.00483.x

Dobrzhinetskaya, L., Green, H. W., & Wang, S. (1996). Alpe Arami: A peridotite massif from depths of more than 300 kilometers. *Science*, *271*(5257), 1841–1845.

Engi, M., Berger, A., & Roselle, G. T. (2001). Role of the tectonic accretion channel in collisional orogeny. *Geology*, *29*(12), 1143–1146. https://doi.org/10.1130/0091-7613(2001)029<1143:ROTTAC>2.0.CO;2

England, P., & Holland, T. (1979). Archimedes and the Tauern eclogites: The role of buoyancy in the preservation of exotic eclogite blocks. *Earth and Planetary Science Letters*, *44*(2), 287–294. https://doi.org/10.1016/0012-821X(79)90177-8

Evans, B. W., & Trommsdorff, V. (1974). Stability of enstatite+ talc, and CO_2-metasomatism of metaperidotite, Val d'Efra, Lepontine Alps. *American Journal of Science*, *274*(3), 274–296. https://doi.org/10.2475/ajs.274.3.274

Evans, B. W., & Trommsdorff, V. (1978). Petrogenesis of garnet lherzolite, Cima di Gagnone, Lepontine Alps. *Earth and Planetary Science Letters*, *40*(3), 333–348. https://doi.org/10.1016/0012-821X(78)90158-9

Evans, B. W., Trommsdorff, V., & Goles, G. G. (1981). Geochemistry of high-grade eclogites and metarodingites from the Central Alps.

Contributions to Mineralogy and Petrology, *76*(3), 301–311. https://doi.org/10.1007/BF00375457

Evans, B., Trommsdorff, V., & Richter, W. (1979). Petrology of an eclogite-metarodingite suite at Cima di Gagnone, Ticino, Switzerland. *American Mineralogist*, *64*(1–2), 15–31.

Federico, L., Crispini, L., Scambelluri, M., & Capponi, G. (2007). Ophiolite mélange zone records exhumation in a fossil subduction channel. *Geology*, *35*(6), 499–502. https://doi.org/10.1130/G23190A.1

Froitzheim, N., Pleuger, J., Roller, S., & Nagel, T. (2003). Exhumation of high-and ultrahigh-pressure metamorphic rocks by slab extraction. *Geology*, *31*(10), 925–928. https://doi.org/10.1130/G19748.1

Froitzheim, N., Schmid, S. M., & Frey, M. (1996). Mesozoic paleogeography and the timing of eclogite-facies metamorphism in the Alps: A working hypothesis. *Eclogae Geologicae Helvetiae*, *89*(1), 81.

Fuhrman, M. L., & Lindsley, D. H. (1988). Ternary-feldspar modeling and thermometry. *American Mineralogist*, *73*(3–4), 201–215.

Gebauer, D. (1996). A PTt Path for an (ultra?-) high-pressure uitramafic/mafic rock-association and its felsic country-rocks based on SHRIMP-dating of magmatic and metamorphic zircon domains. Example: Alpe Arami (Central Swiss Alps). *Geophysical Monograph-American Geophysical Union*, *95*, 307–330.

Gebauer, D., Grünenfelder, M., Tilton, G., Trommsdorff, V., & Schmid, S. (1992). The geodynamic evolution of garnet-peridotites, garnet-pyroxenites and eclogites of Alpe Arami and Cima di Gagnone (Central Alps) from Early Proterozoic to Oligocene. *Schweizerische Mineralogische Und Petrographische Mitteilungen*, *72*(1), 107–111.

Gebauer, D., Schertl, H.-P., Brix, M., & Schreyer, W. (1997). 35 Ma old ultrahigh-pressure metamorphism and evidence for very rapid exhumation in the Dora Maira Massif, Western Alps. *Lithos*, *41*(1–3), 5–24. https://doi.org/10.1016/S0024-4937(97)82002-6

Gerya, T. V., Stöckhert, B., & Perchuk, A. L. (2002). Exhumation of high-pressure metamorphic rocks in a subduction channel: A numerical simulation. *Tectonics*, *21*(6), 6-1–6-19. https://doi.org/10.1029/2002TC001406

Giuntoli, F., Lanari, P., & Engi, M. (2018). Deeply subducted continental fragments–Part 1: Fracturing, dissolution–precipitation, and diffusion processes recorded by garnet textures of the central Sesia Zone (western Italian Alps). *Solid Earth*, *9*(1), 167. https://doi.org/10.5194/se-9-167-2018

Green, E., Holland, T., & Powell, R. (2007). An order-disorder model for omphacitic pyroxenes in the system jadeite-diopside-hedenbergite-acmite, with applications to eclogitic rocks. *American Mineralogist*, *92*(7), 1181–1189. https://doi.org/10.2138/am.2007.2401

Green, H. W., Dobrzhinetskaya, L. F., & Bozhilov, K. N. (2010). The Alpe Arami story: Triumph of data over prejudice. *Journal of Earth Science*, *21*(5), 731–743. https://doi.org/10.1007/s12583-010-0130-0

Grond, R., Wahl, F., & Pfiffner, M. (1995). Mehrphasige alpine deformation und metamorphose in der nördlichen Cima-Lunga-Einheit, Zentralalpen (Schweiz). *Schweizerische Mineralogische Und Petrographische Mitteilungen*, *75*, 371–386.

Guillot, S., Hattori, K. H., de Sigoyer, J., Nägler, T., & Auzende, A.-L. (2001). Evidence of hydration of the mantle wedge and its role in the exhumation of eclogites. *Earth and Planetary Science Letters*, *193*(1–2), 115–127. https://doi.org/10.1016/S0012-821X(01)00490-3

Hacker, B. R., & Gerya, T. V. (2013). Paradigms, new and old, for ultrahigh-pressure tectonism. *Tectonophysics*, *603*, 79–88. https://doi.org/10.1016/j.tecto.2013.05.026

Harlow, G. E., Hemming, S. R., Lallemant, H. G. A., Sisson, V. B., & Sorensen, S. S. (2004). Two high-pressure–low-temperature serpentinite-matrix mélange belts, Motagua fault zone, Guatemala: A record of Aptian and Maastrichtian collisions. *Geology*, *32*(1), 17–20. https://doi.org/10.1130/G19990.1

Harvey, J., Savov, I. P., Agostini, S., Cliff, R. A., & Walshaw, R. (2014). Si-metasomatism in serpentinized peridotite: The effects of talc-alteration on strontium and boron isotopes in abyssal serpentinites from Hole 1268a, ODP Leg 209. *Geochimica et Cosmochimica Acta*, *126*, 30–48. https://doi.org/10.1016/j.gca.2013.10.035

Hattori, K. H., & Guillot, S. (2007). Geochemical character of serpentinites associated with high-to ultrahigh-pressure metamorphic rocks in the Alps, Cuba, and the Himalayas: Recycling of elements in subduction zones. *Geochemistry, Geophysics, Geosystems*, *8*(9). https://doi.org/10.1029/2007GC001594

Heinrich, C. A. (1982). Kyanite-eclogite to amphibolite fades evolution of hydrous mafic and pelitic rocks, Adula nappe, Central Alps. *Contributions to Mineralogy and Petrology*, *81*(1), 30–38. https://doi.org/10.1007/BF00371156

Heinrich, C. (1986). Eclogite facies regional metamorphism of hydrous mafic rocks in the Central Alpine Adula Nappe. *Journal of Petrology*, *27*(1), 123–154. https://doi.org/10.1093/petrology/27.1.123

Hellstrom, J., Paton, C., Woodhead, J., & Hergt, J. (2008). Iolite: Software for spatially resolved LA-(quad and MC) ICPMS analysis. *Mineralogical Association of Canada Short Course Series*, *40*, 343–348.

Hermann, J. (2003). Experimental evidence for diamond-facies metamorphism in the Dora-Maira massif. *Lithos*, *70*(3–4), 163–182.

Hermann, J., & Green, D. H. (2001). Experimental constraints on high pressure melting in subducted crust. *Earth and Planetary Science Letters*, *188*(1–2), 149–168. https://doi.org/10.1016/S0012-821X(01)00321-1

Hermann, J., Müntener, O., & Scambelluri, M. (2000). The importance of serpentinite mylonites for subduction and exhumation of oceanic crust. *Tectonophysics*, *327*(3–4), 225–238. https://doi.org/10.1016/S0040-1951(00)00171-2

Hermann, J., & Rubatto, D. (2009). Accessory phase control on the trace element signature of sediment melts in subduction zones. *Chemical Geology*, *265*(3–4), 512–526. https://doi.org/10.1016/j.chemgeo.2009.05.018

Hermann, J., Rubatto, D., & Trommsdorff, V. (2006). Sub-solidus Oligocene zircon formation in garnet peridotite during fast decompression and fluid infiltration (Duria, Central Alps). *Mineralogy and Petrology*, *88*(1–2), 181–206. https://doi.org/10.1007/s00710-006-0155-3

Hermann, J., & Spandler, C. J. (2008). Sediment melts at sub-arc depths: An experimental study. *Journal of Petrology*, *49*(4), 717–740. https://doi.org/10.1093/petrology/egm073

Herwartz, D., Nagel, T. J., Münker, C., Scherer, E. E., & Froitzheim, N. (2011). Tracing two orogenic cycles in one eclogite sample by Lu–Hf garnet chronometry. *Nature Geoscience*, *4*(3), 178–183. https://doi.org/10.1038/ngeo1060

Holland, T., & Powell, R. (1996). Thermodynamics of order-disorder in minerals: II. Symmetric formalism applied to solid solutions. *American Mineralogist*, *81*(11–12), 1425–1437.

Holland, T. J. B., & Powell, R. (1998). An internally consistent thermodynamic data set for phases of petrological interest. *Journal of Metamorphic Geology*, *16*(3), 309–343. https://doi.org/10.1111/j.1525-1314.1998.00140.x

Holness, M. B., Cesare, B., & Sawyer, E. W. (2011). Melted rocks under the microscope: Microstructures and Their Interpretation. *Elements*, *7*(4), 247–252. https://doi.org/10.2113/gselements.7.4.247

Irouschek, A. (1980). Zur Verbreitung von Cordierit im zentralen Lepontin.

Janots, E., Engi, M., Berger, A., Allaz, J., Schwarz, J., & Spandler, C. (2008). Prograde metamorphic sequence of REE minerals in pelitic rocks of the Central Alps: Implications for allanite–monazite–xenotime phase relations from 250 to 610 C. *Journal of Metamorphic Geology*, *26*(5), 509–526.

Jolivet, L., Raimbourg, H., Labrousse, L., Avigad, D., Leroy, Y., Austrheim, H., & Andersen, T. B. (2005). Softening trigerred by eclogitization, the first step toward exhumation during continental subduction. *Earth and Planetary Science Letters*, *237*(3–4), 532–547. https://doi.org/10.1016/j.epsl.2005.06.047

Kästle, E. D., Rosenberg, C., Boschi, L., Bellahsen, N., Meier, T., & El-Sharkawy, A. (2020). Slab break-offs in the Alpine subduction zone. *International Journal of Earth Sciences*, *109*(2), 587–603. https://doi.org/10.1007/s00531-020-01821-z

Kawakami, T., Yamaguchi, I., Miyake, A., Shibata, T., Maki, K., Yokoyama, T. D., & Hirata, T. (2013). Behavior of zircon in the upper-amphibolite to granulite facies schist/migmatite transition, Ryoke metamorphic belt, SW Japan: Constraints from the melt inclusions in zircon. *Contributions to Mineralogy and Petrology*, *165*(3), 575–591. https://doi.org/10.1007/s00410-012-0824-7

Kissling, E., & Schlunegger, F. (2018). Rollback orogeny model for the evolution of the Swiss Alps. *Tectonics*, *37*(4), 1097–1115. https://doi.org/10.1002/2017TC004762

Krebs, M., Schertl, H.-P., Maresch, W., & Draper, G. (2011). Mass flow in serpentinite-hosted subduction channels: P-T–t path patterns of metamorphic blocks in the Rio San Juan mélange (Dominican Republic). *Journal of Asian Earth Sciences*, *42*(4), 569–595. https://doi.org/10.1016/j.jseaes.2011.01.011

Lanari, P., & Engi, M. (2017). Local bulk composition effects on metamorphic mineral assemblages. *Reviews in Mineralogy and Geochemistry*, *83*(1), 55–102. https://doi.org/10.2138/rmg.2017.83.3

Lanari, P., & Hermann, J. (2020). Iterative thermodynamic modelling—Part 2: Tracing equilibrium relationships between minerals in metamorphic rocks. *Journal of Metamorphic Geology*, 1–24. https://doi.org/10.1111/jmg.12575

Lanari, P., & Piccoli, F. (2020). New horizons in quantitative compositional mapping–Analytical conditions and data reduction using XMapTools, Vol. 891, p. 012016. IOP Publishing.

Lanari, P., Vho, A., Bovay, T., Airaghi, L., & Centrella, S. (2019). Quantitative compositional mapping of mineral phases by electron probe micro-analyser. *Geological Society, London, Special Publications*, *478*(1), 39–63. https://doi.org/10.1144/SP478.4

Lanari, P., Vidal, O., De Andrade, V., Dubacq, B., Lewin, E., Grosch, E. G., & Schwartz, S. (2014). XMapTools: A MATLAB©-based program for electron microprobe X-ray image processing and geothermobarometry. *Computers & Geosciences*, *62*, 227–240. https://doi.org/10.1016/j.cageo.2013.08.010

Lang, H., & Gilotti, J. (2007). Partial melting of metapelites at ultrahigh-pressure conditions, Greenland Caledonides. *Journal of Metamorphic Geology*, *25*(2), 129–147. https://doi.org/10.1111/j.1525-1314.2006.00687.x

Lang, H. M., & Gilotti, J. A. (2015). Modeling the exhumation path of partially melted ultrahigh-pressure metapelites, North-East Greenland Caledonides. *Lithos*, *226*, 131–146. https://doi.org/10.1016/j.lithos.2014.10.010

Liati, A., Gebauer, D., & Fanning, C. M. (2009). Geochronological evolution of HP metamorphic rocks of the Adula nappe, Central Alps, in pre-Alpine and Alpine subduction cycles. *Journal of the Geological Society*, *166*(4), 797–810. https://doi.org/10.1144/0016-76492008-033

Luisier, C., Baumgartner, L., Schmalholz, S. M., Siron, G., & Vennemann, T. (2019). Metamorphic pressure variation in a coherent Alpine nappe challenges lithostatic pressure paradigm. *Nature Communications*, *10*(1), 1–11. https://doi.org/10.1038/s41467-019-12727-z

Lundin, E. R., & Doré, A. G. (2011). Hyperextension, serpentinization, and weakening: A new paradigm for rifted margin compressional deformation. *Geology*, *39*(4), 347–350. https://doi.org/10.1130/G31499.1

Majka, J., Rosén, Å., Janák, M., Froitzheim, N., Klonowska, I., Manecki, M., Sasinková, V., & Yoshida, K. (2014). Microdiamond discovered in the Seve Nappe (Scandinavian Caledonides) and its exhumation by the "vacuum-cleaner" mechanism. *Geology*, *42*(12), 1107–1110. https://doi.org/10.1130/G36108.1

Marschall, H. R., Dohmen, R., & Ludwig, T. (2013). Diffusion-induced fractionation of niobium and tantalum during continental crust formation. *Earth and Planetary Science Letters*, *375*, 361–371. https://doi.org/10.1016/j.epsl.2013.05.055

Maxelon, M., & Mancktelow, N. S. (2005). Three-dimensional geometry and tectonostratigraphy of the Pennine zone, Central Alps, Switzerland and Northern Italy. *Earth-science Reviews*, *71*(3–4), 171–227. https://doi.org/10.1016/j.earscirev.2005.01.003

Meyre, C., De Capitani, C., Zack, T., & Frey, M. (1999). Petrology of high-pressure metapelites from the Adula nappe (Central Alps, Switzerland). *Journal of Petrology*, *40*(1), 199–213. https://doi.org/10.1093/petroj/40.1.199

Meyre, C., & Puschnig, A. (1993). High-pressure metamorphism and deformation at Trescolmen, Adula nappe, Central Alps. *Schweizerische Mineralogische Und Petrographische Mitteilungen*, *73*(2), 277–283.

Mohn, G., Manatschal, G., Masini, E., & Müntener, O. (2011). Rift-related inheritance in orogens: A case study from the Austroalpine nappes in Central Alps (SE-Switzerland and N-Italy). *International Journal of Earth Sciences*, *100*(5), 937–961. https://doi.org/10.1007/s00531-010-0630-2

Moulas, E., Podladchikov, Y. Y., Aranovich, L. Y., & Kostopoulos, D. (2013). The problem of depth in geology: When pressure does not translate into depth. *Petrology*, *21*(6), 527–538. https://doi.org/10.1134/S0869591113060052

Nagel, T. J. (2008). Tertiary subduction, collision and exhumation recorded in the Adula nappe, central Alps. *Geological Society, London, Special Publications*, *298*(1), 365–392. https://doi.org/10.1144/SP298.17

Nimis, P., & Trommsdorff, V. (2001). Revised Thermobarometry of Alpe Arami and other garnet peridotites from the Central Alps. *Journal of Petrology*, *42*(1), 103–115. https://doi.org/10.1093/petrology/42.1.103

Nimis, P., Trommsdorff, V., & Russo, U. (1999). Revised thermobarometry of Grt-peridotites from Cima Lunga-Adula nappe complex, Central Alps. *Ofioliti*, *24*(1b), 143–144.

Paquin, J., & Altherr, R. (2001). New Constraints on the P-T evolution of the Alpe Arami garnet peridotite body (Central Alps, Switzerland). *Journal of Petrology*, *42*(6), 1119–1140. https://doi.org/10.1093/petrology/42.6.1119

Paton, C., Hellstrom, J., Paul, B., Woodhead, J., & Hergt, J. (2011). Iolite: Freeware for the visualisation and processing of mass spectrometric data. *Journal of Analytical Atomic Spectrometry*, *26*(12), 2508–2518. https://doi.org/10.1039/c1ja10172b

Perchuk, A. L., Burchard, M., Maresch, W. V., & Schertl, H. (2005). Fluid-mediated modification of garnet interiors under ultrahigh-pressure conditions. *Terra Nova*, *17*(6), 545–553. https://doi.org/10.1111/j.1365-3121.2005.00647.x

Pfiffner, M. A. (1999). Genese der hochdruckmetamorphen ozeanischen Abfolge der Cima Lunga-Einheit (Zentralalpen).

Pfiffner, M., & Trommsdorff, V. (1998). The high-pressure ultramafic-mafic-carbonate suite of Cima Lunga-Adula, Central Alps: Excursions to Cima di Gagnone and Alpe Arami. *Schweizerische Mineralogische Und Petrographische Mitteilungen*, *78*(2), 337–354.

Piccoli, F., Hermann, J., Pettke, T., Connolly, J., Kempf, E. D., & Duarte, J. V. (2019). Subducting serpentinites release reduced, not oxidized, aqueous fluids. *Scientific Reports*, *9*(1), 1–7. https://doi.org/10.1038/s41598-019-55944-8

Pleuger, J., & Podladchikov, Y. Y. (2014). A purely structural restoration of the NFP20-East cross section and potential tectonic overpressure in the Adula nappe (central Alps). *Tectonics*, *33*(5), 656–685. https://doi.org/10.1002/2013TC003409

Raimondo, T., Payne, J., Wade, B., Lanari, P., Clark, C., & Hand, M. (2017). Trace element mapping by LA-ICP-MS: Assessing geochemical mobility in garnet. *Contributions to Mineralogy and Petrology*, *172*(4), 17. https://doi.org/10.1007/s00410-017-1339-z

Rice, J. M., Evans, B. W., & Trommsdorff, V. (1974). Widespread occurrence of magnesiocummingtonite in ultramafic schists, Cima di Gagnone, Ticino, Switzerland. *Contributions to Mineralogy and Petrology*, *43*(4), 245–251. https://doi.org/10.1007/BF00373481

Robyr, M., Darbellay, B., & Baumgartner, L. (2014). Matrix-dependent garnet growth in polymetamorphic rocks of the Sesia zone, Italian Alps. *Journal of Metamorphic Geology*, *32*(1), 3–24. https://doi.org/10.1111/jmg.12055

Rubatto, D., Burger, M., Lanari, P., Hattendorf, B., Schwarz, G., Neff, C., Keresztes Schmidt, P., Hermann, J., Vho, A., & Günther, D. (2020). Identification of growth mechanisms in metamorphic garnet by high-resolution trace element mapping with LA-ICP-TOFMS. *Contributions to Mineralogy and Petrology*, *175*(61), 61. https://doi.org/10.1007/s00410-020-01700-5

Rubatto, D., Gebauer, D., & Fanning, M. (1998). Jurassic formation and Eocene subduction of the Zermatt–Saas-Fee ophiolites: Implications for the geodynamic evolution of the Central and Western Alps. *Contributions to Mineralogy and Petrology*, *132*(3), 269–287. https://doi.org/10.1007/s004100050421

Rubatto, D., Hermann, J., Berger, A., & Engi, M. (2009). Protracted fluid-induced melting during Barrovian metamorphism in the Central Alps. *Contributions to Mineralogy and Petrology*, *158*(6), 703–722. https://doi.org/10.1007/s00410-009-0406-5

Rubatto, D., Regis, D., Hermann, J., Boston, K., Engi, M., Beltrando, M., & McAlpine, S. R. (2011). Yo-yo subduction recorded by accessory minerals in the Italian Western Alps. *Nature Geoscience*, *4*(5), 338–342. https://doi.org/10.1038/ngeo1124

Salters, V. J., & Stracke, A. (2004). Composition of the depleted mantle. *Geochemistry, Geophysics, Geosystems*, *5*(5). https://doi.org/10.1029/2003GC000597

Scambelluri, M., Pettke, T., & Cannaò, E. (2015). Fluid-related inclusions in Alpine high-pressure peridotite reveal trace element recycling during subduction-zone dehydration of serpentinized mantle (Cima di Gagnone, Swiss Alps). *Earth and Planetary Science Letters*, *429*, 45–59. https://doi.org/10.1016/j.epsl.2015.07.060

Scambelluri, M., Pettke, T., Rampone, E., Godard, M., & Reusser, E. (2014). Petrology and trace element budgets of high-pressure peridotites indicate subduction dehydration of serpentinized mantle (Cima di Gagnone, Central Alps, Switzerland). *Journal of Petrology*, *55*(3), 459–498. https://doi.org/10.1093/petrology/egt068

Schenker, F. L., Ambrosi, C., Scapozza, C., Czerski, D., Maino, M., & Castelletti, C. (2019). Rheological inheritance vs. disruptive tectonics: On the lithological incoherence of the high pressure (HP) Cima Lunga Unit (Central Alps). In *Geophysical Research Abstracts* (Vol. 21).

Schenker, F. L., Schmalholz, S. M., Moulas, E., Pleuger, J., Baumgartner, L. P., Podladchikov, Y., Vrijmoed, J., Buchs, N., & Müntener, O. (2015). Current challenges for explaining (ultra) high-pressure tectonism in the Pennine domain of the Central and Western Alps. *Journal of Metamorphic Geology*, *33*(8), 869–886. https://doi.org/10.1111/jmg.12143

Schmalholz, S., & Duretz, T. (2015). Shear zone and nappe formation by thermal softening, related stress and temperature evolution, and application to the Alps. *Journal of Metamorphic Geology*, *33*(8), 887–908. https://doi.org/10.1111/jmg.12137

Schmalholz, S. M., Duretz, T., Schenker, F. L., & Podladchikov, Y. Y. (2014). Kinematics and dynamics of tectonic nappes: 2-D numerical modelling and implications for high and ultra-high pressure tectonism in the Western Alps. *Tectonophysics*, *631*, 160–175. https://doi.org/10.1016/j.tecto.2014.05.018

Snow, J. E., Hart, S. R., & Dick, H. J. (1993). Orphan strontium-87 in abyssal peridotites: Daddy was a granite. *Science-AAAS-Weekly Paper Edition-Including Guide to Scientific Information*, *262*(5141), 1861–1863.

Spandler, C., Yaxley, G., Green, D. H., & Scott, D. (2010). Experimental phase and melting relations of metapelite in the upper mantle: Implications for the petrogenesis of intraplate magmas. *Contributions to Mineralogy and Petrology*, *160*(4), 569–589. https://doi.org/10.1007/s00410-010-0494-2

Stepanov, A. S., Hermann, J., Rubatto, D., Korsakov, A. V., & Danyushevsky, L. V. (2016). Melting history of an ultrahigh-pressure paragneiss revealed by multiphase solid inclusions in garnet, Kokchetav massif, Kazakhstan. *Journal of Petrology*, *57*(8), 1531–1554. https://doi.org/10.1093/petrology/egw049

Stepanov, A. S., Rubatto, D., Hermann, J., & Korsakov, A. V. (2016). Contrasting PT paths within the Barchi-Kol UHP terrain (Kokchetav Complex): Implications for subduction and exhumation of continental crust. *American Mineralogist*, *101*(4), 788–807.

Syracuse, E. M., van Keken, P. E., & Abers, G. A. (2010). The global range of subduction zone thermal models. *Physics of the Earth and Planetary Interiors*, *183*(1–2), 73–90.

Tajčmanová, L., Connolly, J., & Cesare, B. (2009). A thermodynamic model for titanium and ferric iron solution in biotite. *Journal of Metamorphic Geology*, *27*(2), 153–165. https://doi.org/10.1111/j.1525-1314.2009.00812.x

Tajčmanová, L., Podladchikov, Y., Powell, R., Moulas, E., Vrijmoed, J., & Connolly, J. (2014). Grain-scale pressure variations and chemical equilibrium in high-grade metamorphic rocks. *Journal of Metamorphic Geology*, *32*(2), 195–207. https://doi.org/10.1111/jmg.12066

Tajčmanová, L., Vrijmoed, J., & Moulas, E. (2015). Grain-scale pressure variations in metamorphic rocks: Implications for the interpretation of petrographic observations. *Lithos*, *216*, 338–351. https://doi.org/10.1016/j.lithos.2015.01.006

Todd, C., & Engi, M. (1997). Metamorphic field gradients in the Central Alps. *Journal of Metamorphic Geology*, *15*(4), 513–530. https://doi.org/10.1111/j.1525-1314.1997.00038.x

Tomkins, H., Powell, R., & Ellis, D. (2007). The pressure dependence of the zirconium-in-rutile thermometer. *Journal of Metamorphic Geology*, *25*(6), 703–713. https://doi.org/10.1111/j.1525-1314.2007.00724.x

Toóth, T., Grandjean, V., & Engi, M. (2000). Polyphase evolution and reaction sequence of compositional domains in metabasalt: A model based on local chemical equilibrium and metamorphic differentiation. *Geological Journal*, *35*(3–4), 163–183.

Trommsdorff, V. (1990). Metamorphism and tectonics in the Central Alps: The Alpine lithospheric mélange of Cima Lunga and Adula. *Memorie Della Società Geologica Italiana*, *45*, 39–49.

Trommsdorff, V., Hermann, J., Müntener, O., Pfiffner, M., & Risold, A.-C. (2000). Geodynamic cycles of subcontinental lithosphere in the Central Alps and the Arami enigma. *Journal of Geodynamics*, *30*(1–2), 77–92. https://doi.org/10.1016/S0264-3707(99)00028-9

Tumiati, S., Zanchetta, S., Pellegrino, L., Ferrario, C., Casartelli, S., & Malaspina, N. (2018). Granulite-facies overprint in garnet peridotites and kyanite eclogites of Monte Duria (Central Alps, Italy): Clues from srilankite-and sapphirine-bearing symplectites. *Journal of Petrology*, *59*(1), 115–151. https://doi.org/10.1093/petrology/egy021

Vitale Brovarone, A., Beltrando, M., Malavieille, J., Giuntoli, F., Tondella, E., Groppo, C., Beyssac, O., & Compagnoni, R. (2011). Inherited Ocean-Continent Transition zones in deeply subducted terranes: Insights from Alpine Corsica. *Lithos*, *124*(3–4), 273–290. https://doi.org/10.1016/j.lithos.2011.02.013

von Blanckenburg, F., & Davies, J. H. (1995). Slab breakoff: A model for syncollisional magmatism and tectonics in the Alps. *Tectonics*, *14*(1), 120–131. https://doi.org/10.1029/94TC02051

Warren, C., Beaumont, C., & Jamieson, R. A. (2008). Modelling tectonic styles and ultra-high pressure (UHP) rock exhumation during the transition from oceanic subduction to continental collision. *Earth and Planetary Science Letters*, *267*(1–2), 129–145. https://doi.org/10.1016/j.epsl.2007.11.025

Wenk, E. (1955). Eine Strukturkarte der Tessineralpen. Verlag nicht ermittelbar.

White, R., Powell, R., & Holland, T. (2001). Calculation of partial melting equilibria in the system Na_2O–CaO–K_2O–FeO–MgO–Al_2O_3–SiO_2–H_2O (NCKFMASH). *Journal of Metamorphic Geology*, *19*(2), 139–153.

Woodhead, J. D., Hellstrom, J., Hergt, J. M., Greig, A., & Maas, R. (2007). Isotopic and elemental imaging of geological materials by laser ablation inductively coupled plasma-mass spectrometry. *Geostandards and Geoanalytical Research*, *31*(4), 331–343. https://doi.org/10.1111/j.1751-908X.2007.00104.x

SUPPORTING INFORMATION

Additional supporting information may be found online in the Supporting Information section.

Appendix S1: electron microprobe spot analysis.

Table S1.1. Garnet EPMA analyses.

Table S1.2. White mica EPMA analyses.

Table S1.3. Kyanite EPMA analyses.

Table S1.4. Biotite EPMA analyses.

Table S1.5. Plagioclase EPMA analyses

Appendix S2: analytical conditions and data of LA-ICP-MS analyses.

Table S2.1 LA-ICP-MS garnet mapping and spot analysis method.

Table S2.2 LA-ICP-MS measurement of garnet trace element composition in μ g/g.

Table S2.3 LA-ICP-MS rutile measurement analytical conditions.

Table S2.4 LA-ICP-MS measurement of rutile trace element composition in μ g/g.

Table S3: mineral modal abundance and calculated local bulk composition per each zone (D1, D2, and D3).

Figure S1: *P–T* phase diagram together with X_{Prp} isopleths (blue lines), Si in phengite isopleths (yellow lines), and Ti in phengite isopleths (green lines).

Figure S2: X-ray micro-computed tomography of the sample highlighting the abundance of atoll-shaped garnet.

How to cite this article: Piccoli, F., Lanari, P., Hermann, J., & Pettke, T. (2022). Deep subduction, melting, and fast cooling of metapelites from the Cima Lunga Unit, Central Alps. *Journal of Metamorphic Geology*, *40*(1), 121–143. https://doi.org/10.1111/jmg.12621